AD-A0[redacted]93 GEORGIA INST OF TECH ATLANTA ENGINEERING EXPERIMENT --ETC F/G 17/9
NEAR MILLIMETER WAVE RADAR TECHNOLOGY.(U)
JAN 80 R W MCMILLAN, R E FORSYTHE DAAK70-79-C-0108

UNCLASSIFIED NL

1 OF 2
AD-
A083493

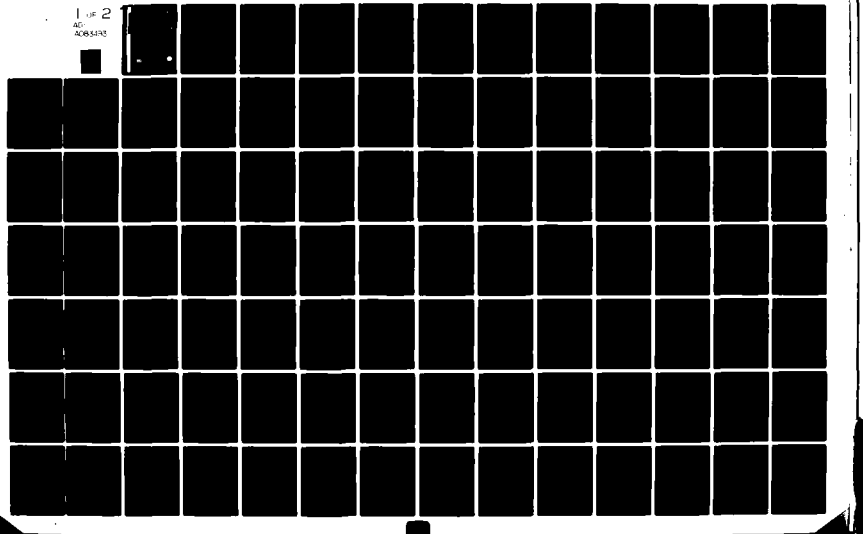

PHASE I INTERIM TECHNICAL REPORT

NEAR MILLIMETER WAVE RADAR TECHNOLOGY

LEVEL II

R. W. McMillan, R. E. Forsythe, R. A. Bohlander,
R. G. Shackelford, R. N. Trebits, W. A. Holm

CONTRACT NO. DAAK70–79–C–0108

11 January 1980

GEORGIA INSTITUTE OF TECHNOLOGY
Engineering Experiment Station
Atlanta, Georgia 30332

GTEES

NEAR MILLIMETER WAVE RADAR TECHNOLOGY

PHASE I INTERIM TECHNICAL REPORT

CONTRACT NO. DAAK70-79-C-0108
(A-2445)

by

R. W. McMillan, R. E. Forsythe, R. A. Bohlander
R. G. Shackelford, R. N. Trebits, W. A. Holm

Georgia Institute of Technology
Engineering Experiment Station
Atlanta, Georgia 30332

Prepared for

U. S. Army Mobility Equipment Research
and Development Command
Night Vision Laboratory
Ft. Belvoir, Virginia 22060

January 11, 1980

TABLE OF CONTENTS

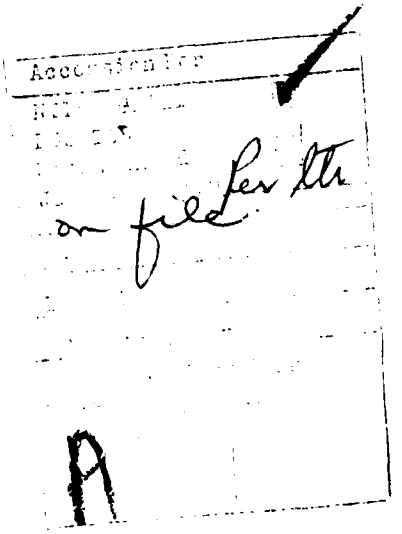

LIST OF FIGURES

PAGE

LIST OF TABLES

1.0 INTRODUCTION

1.1 Background

On November 13, 1979 a review of the proposed design of the 220 GHz near millimeter wave (NMMW) radar system being developed for the U. S. Army Night Vision Laboratory (NVL) by the Engineering Experiment Station of the Georgia Institute of Technology was held at the NVL facility at Fort Belvoir, Virginia. The review was presented by R. E. Forsythe, R. A. Holm, R. N. Trebits, and R. W. McMillan of Georgia Tech, and was attended by personnel from several Army laboratories as well as those from NVL. This report discusses the approaches decided upon for the final design of the system as well as the options considered in arriving at these approaches.

1.2 Purpose of System

With the technology at the lower NMMW frequencies very well developed, it is reasonable to ask why a 220 GHz system should be considered for Army applications. In particular, sources, receivers, and ferrite switches are available for use at both 94 and 140 GHz, while these devices are generally more difficult to obtain and do not perform as well at 220 GHz. Furthermore, the atmospheric window at 220 GHz has higher attenuation of electromagnetic radiation than those at either 94 or 140 GHz under all conditions, thus adding to the disadvantages of the higher frequency system. This section will attempt to answer some of these questions.

The most obvious advantage of the higher frequency system is the reduced antenna size. The half-power beamwidth of an antenna is approximately 1.2 λ/D where λ is wavelength and D is aperture. For a given beamwidth, therefore, the aperture can be scaled downward in size by the ratio of the wavelengths. In scaling upward from 94 to 220 GHz for example, a 15 inch diameter antenna thus becomes a 6 inch diameter antenna. The advantage of this smaller size to a potential user are then very significant. The antenna has significantly less impact on the profile of the vehicle on which it is used, and may resemble a searchlight, for example, rather than an antenna for a sophisticated radar system.

Similarly, for the same size antenna, moving to a higher frequency will reduce the beamwidth and multipath effects. Although the antenna size for the present radar system is constrained to be six inches, the use of a 15 inch diameter antenna with the 220 GHz system would greatly reduce multipath effects. Ground multipath generally causes the apparent target centroid to be depressed because the target image due to ground reflections biases the direct target return. These considerations affect both surveillance and fire control systems. Some improvement in tracking accuracy is also potentially possible with the smaller beamwidth, although this potential increase can be offset by decreased receiver sensitivity and increased atmospheric losses.

Higher frequencies will generally be more covert, due to increased atmospheric absorption, reduced target spillover and added difficulty in detecting shorter wavelengths. Furthermore, off-axis radiation from the radar will fall off more rapidly due to absorption, even though

scattering from fog and aerosols is increasing as frequency to the sixth power. At 220 GHz, scattering from fog is still negligible when compared to absorption. It should therefore be just as difficult to detect a 220 GHz system by using off-axis radiation as it is to detect a lower frequency system by the same means.

To summarize this section, it is probably reasonable to state that the most important reason for building a 220 GHz radar system as compared to a lower frequency system is related to the reduced antenna size and the resulting minimal influence on the profile of vehicles, especially tanks, on which the radar is mounted. A secondary but important consideration is the reduction of multipath and increased resolution afforded by a 220 GHz system with the same size antenna as used with a lower frequency system.

1.3 Overview of System

The proposed system consists of a transmitter, receiver, antenna duplexer, and antenna subsystem. An attempt will be made to phase lock the Varian VKY-2429R EIO transmitter to the receiver local oscillator to give a quasi-coherent system. Quasi-coherent means that the transmitted pulse is coherent near its center and incoherent during rise and fall times. The receiver will be of all solid state design, using an f/4 subharmonic mixer developed at Georgia Tech together with a Hughes 55 GHz phase locked Gunn local oscillator. The antenna duplexer will be an optical subsystem, depending partially for its operation on the change in sense of circular polarization when reflected from a single-bounce target, and partially on the operation of an interferometric switch used for receiver isolation.

The antenna will be a 15 cm (6 inch) lens machined from a piece of TPX plastic, and the beam will be steered by a 2-axis gimbal system being designed by Carson Astronomical Instruments of Albuquerque, N.M. Although there will be no signal processing hardware included in the proposed system, the antenna will have both a raster scan mode for search and a conical scan mode for track. The entire system will be designed to be amenable to the addition of radar signal processing at a later time. Table 1-I summarizes the system parameters and Figure 1-1 is a block diagram of the entire system. Figure 1-2 is a preliminary conceptual drawing of the radar, shown with approximate dimensions. Each of the major subsystems will be treated in some detail in the sections that follow.

1.4 System Weather Performance

The radar range equation was used to calculate [1] the expected system range as a function of signal-to-noise ratio (SNR) for several different weather conditions of interest, including clear dry, 30 m fog, and 4 mm/hr rain. Figure 1-2 shows the result of this calculation for warm dry weather conditions with the other pertinent parameters shown on the figure. Note that the range is about 2.3 km for an SNR of unity with a pulse width of 50 nsec. With the addition of data processing, this SNR is expected to improve to about 15 dB for the same range, which would also manifest itself as a longer range with a lower SNR. Figures 1-3 and 1-4 show the results of similar calculations for a 30 m fog and 4 mm/hr rain, respectively, with the result that the 1 dB SNR range is about 1.3 km in each case.

TABLE 1-I. NEAR MILLIMETER WAVE RADAR SYSTEM SPECIFICATIONS

Operating Frequency	220 GHz
Antenna Aperture	6 inches, diameter
Beam Scan Sector	7.5 degrees elevation x 15 degrees azimuth
Sector Search Time	2 seconds
Range Resolution	± 10 meters
Target Velocities	2 to 50 km/hr, radial
Probability of Detection	90%, 3 km, clear air 90%, 1.5 km, fog

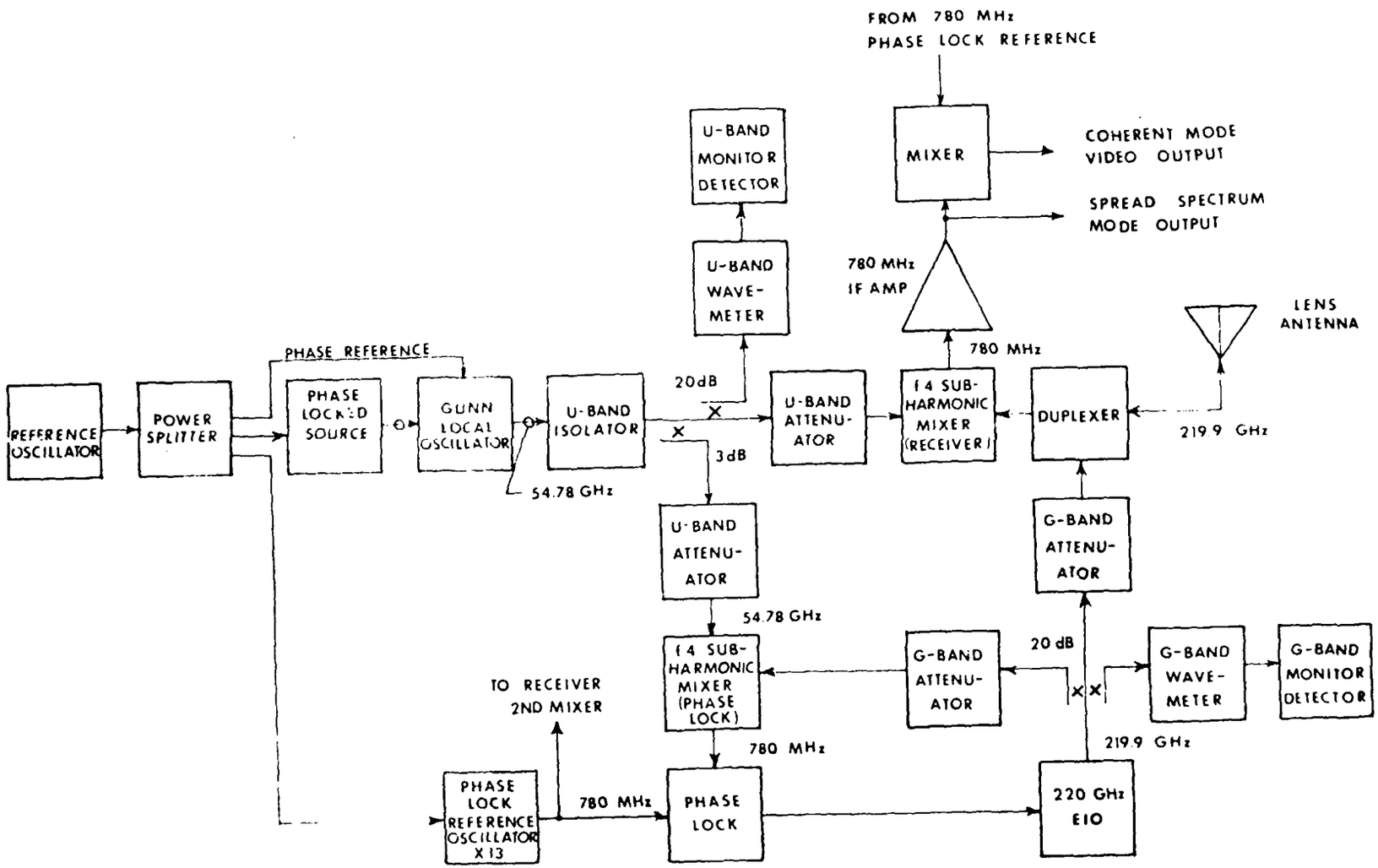

Figure 1-1. 220 GHz NMMW Radar Block Diagram.

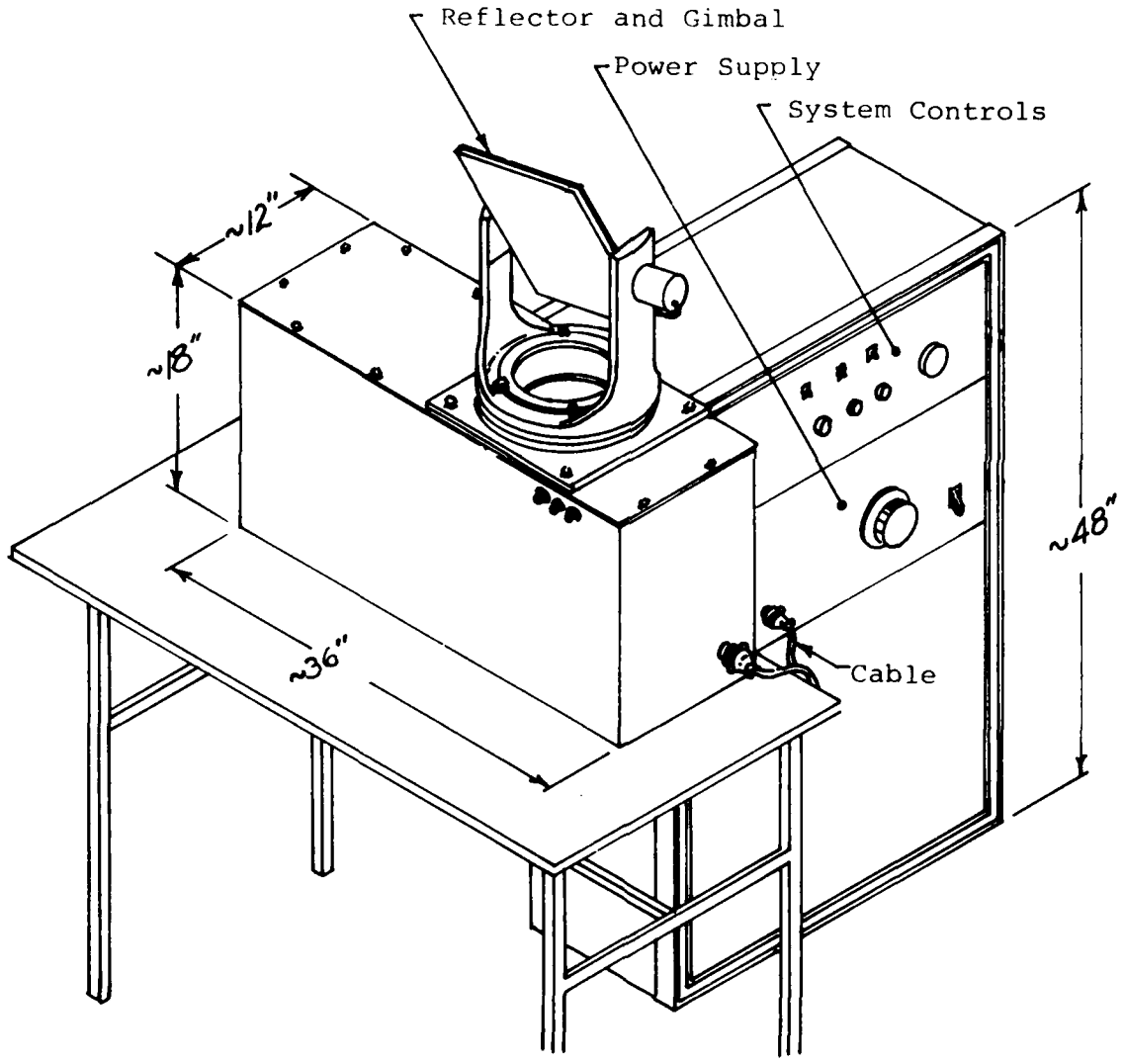

Figure 1-2. Preliminary Conceptual Drawing of the 220 GHz Radar Mechanical Configuration.

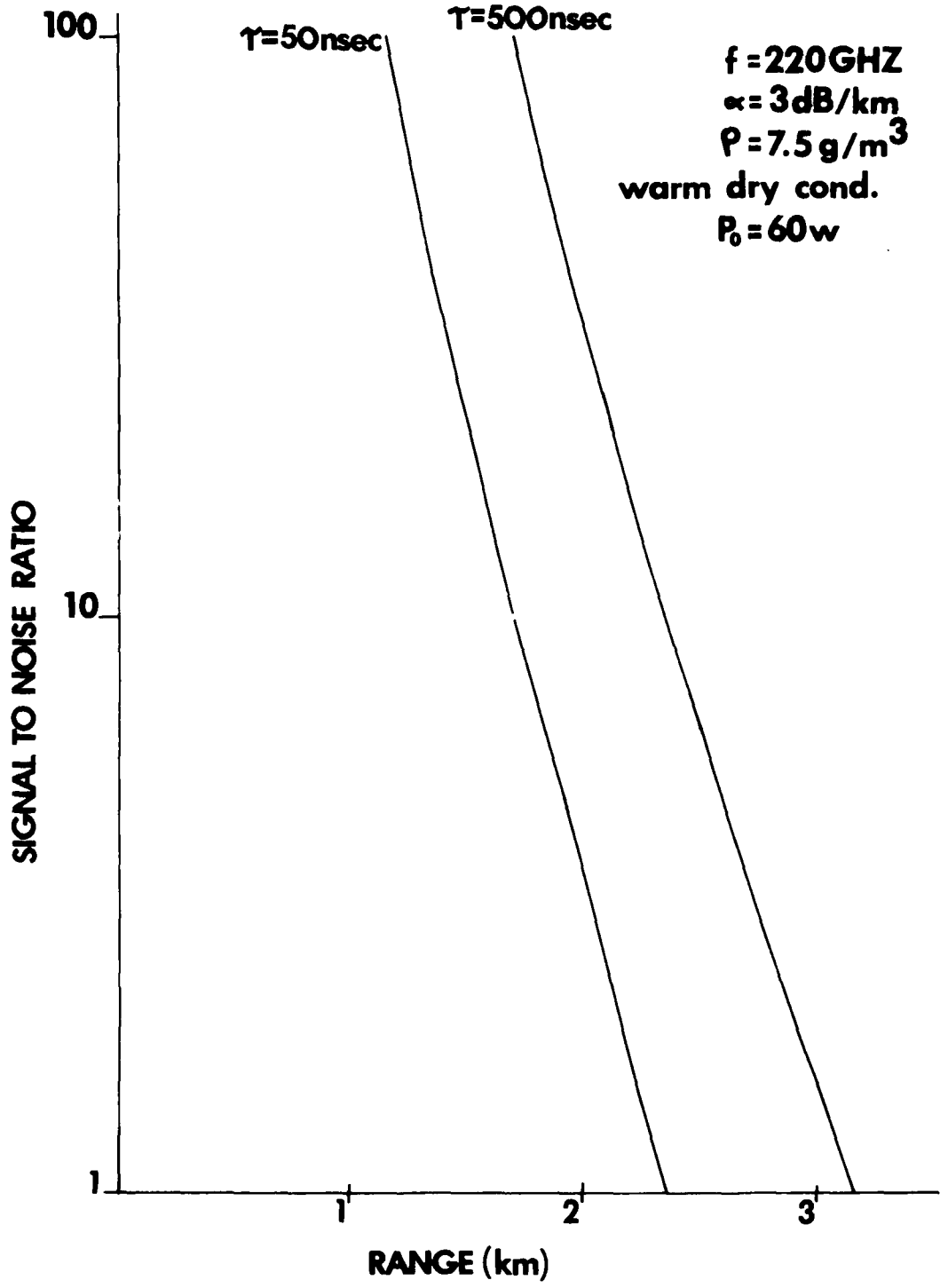

Figure 1-3. Calculated Range of 220 GHz Radar System Under Warm Dry Conditions.

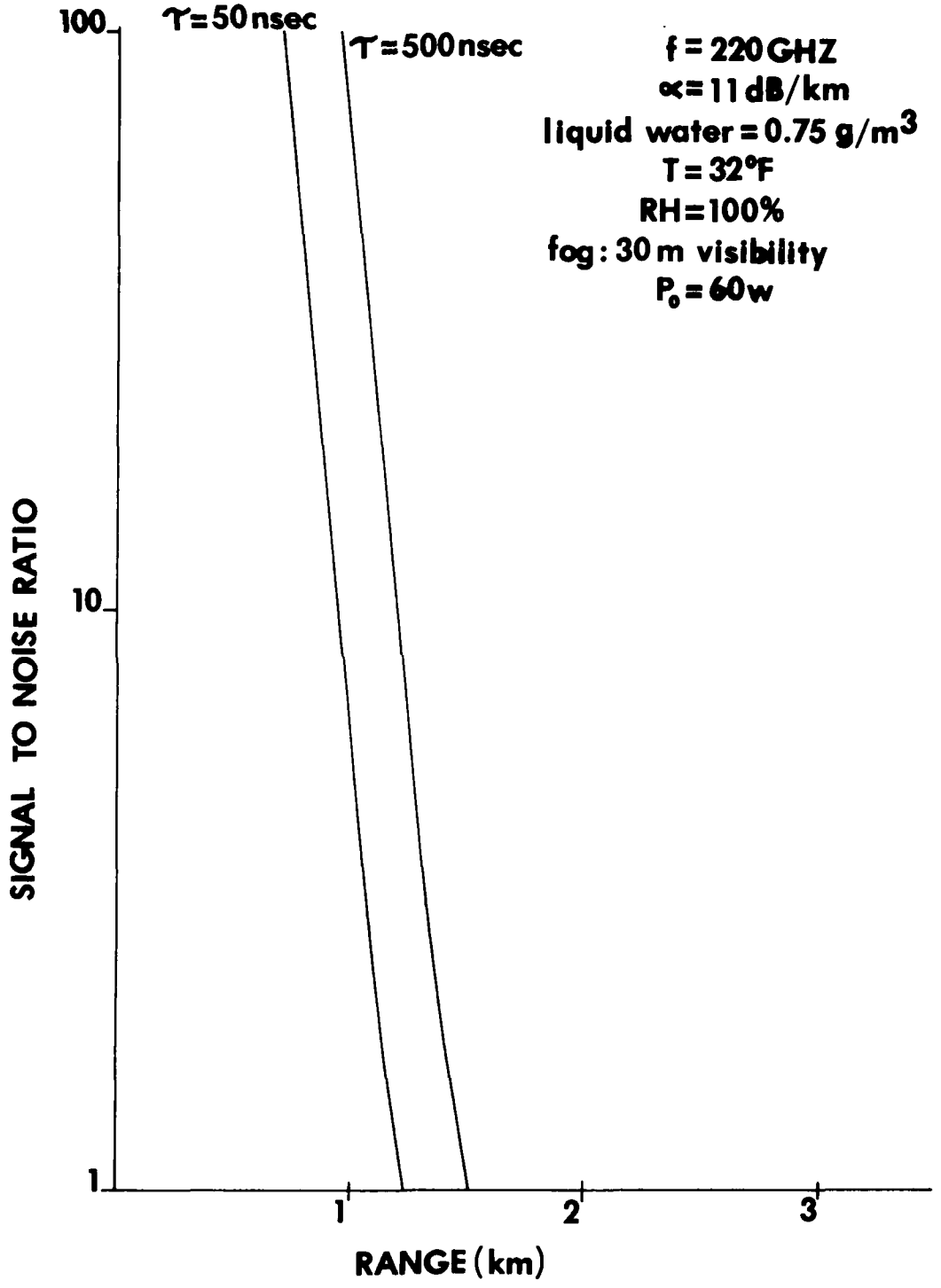

Figure 1-4. Calculated Range of the 220 GHz Radar In a 30 m Visibility Fog.

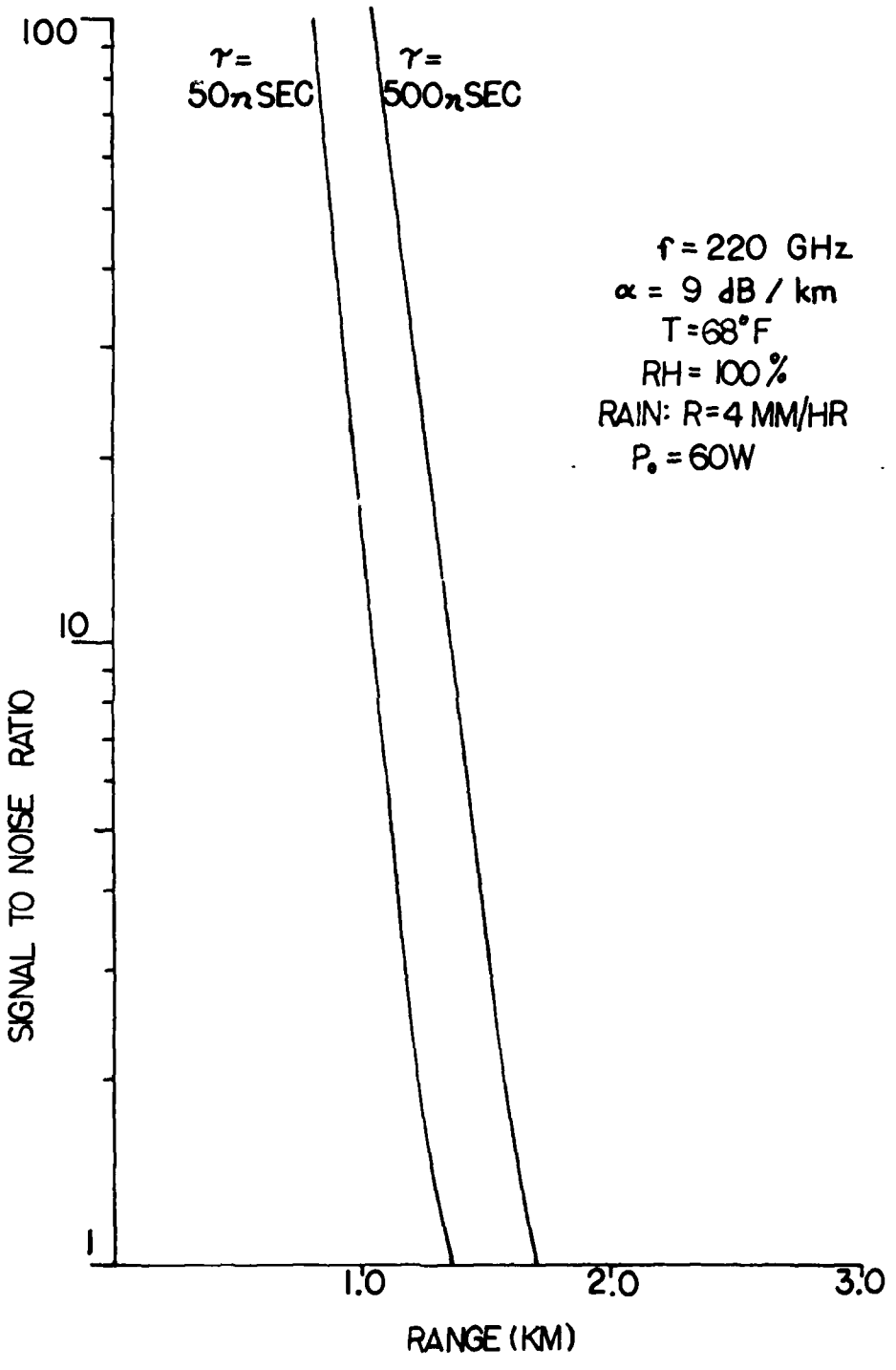

Figure 1-5. Calculated Range of the 220 GHz Radar System in a 4 mm per hour Rainfall.

Since the EIO to be used in this radar transmitter has an output power of only 60 watts, one might expect to be able to increase the range significantly by increasing the power. Figure 1-5 shows that this approach is probably not cost effective, in that doubling the transmitter power for a given SNR only increases the range by about 10% under clear, dry conditions. For weather conditions that are worse, this increase is likely to be even less. These results show that useful tactical ranges can be achieved by using available EIO sources at 220 GHz, but that the 220 GHz atmospheric window is also more susceptible to degradation of atmopsheric parameters in the form of high humidity, rain, and fog than are the lower frequency windows.

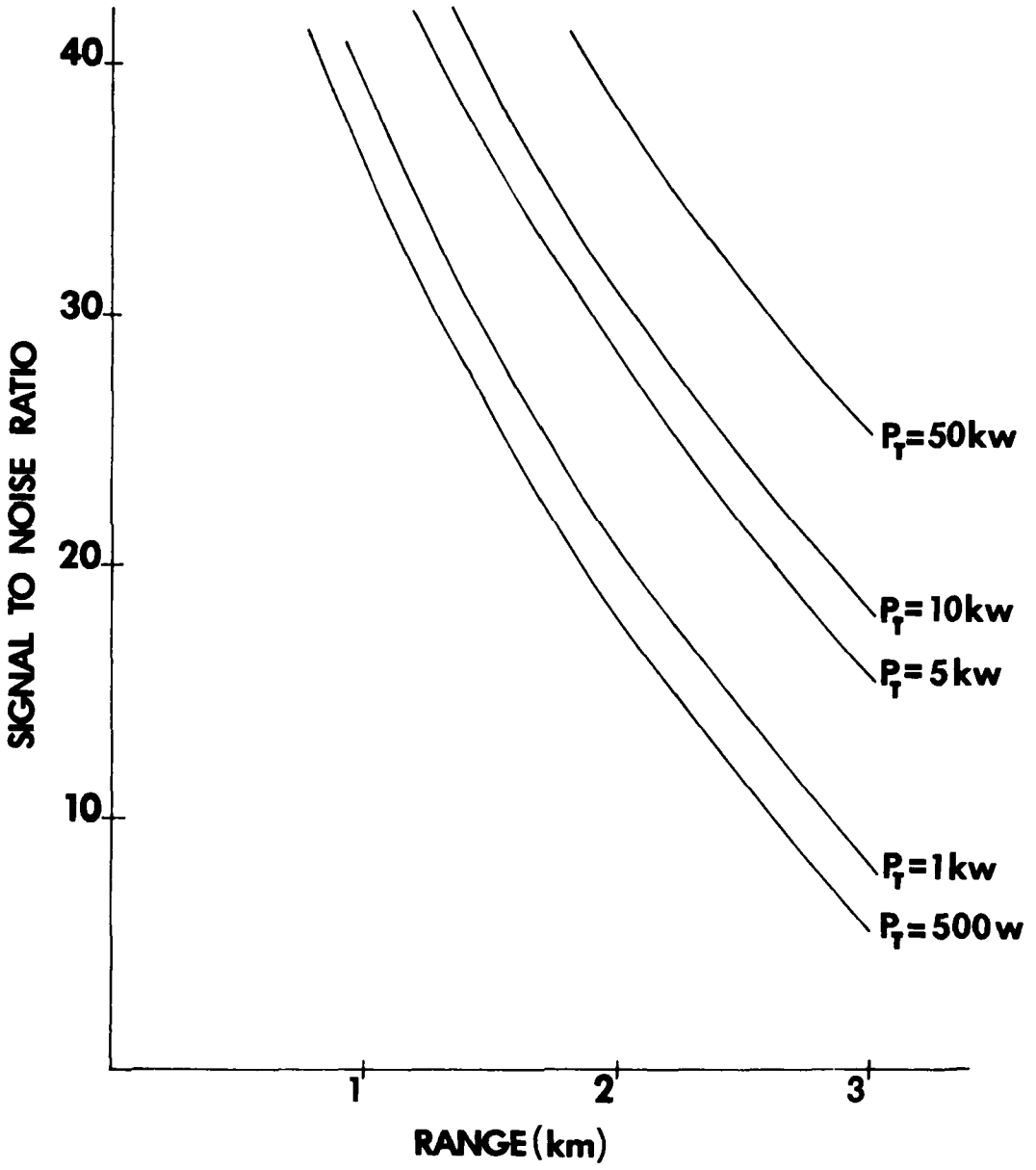

Figure 1-6. Calculated 220 GHz Radar System SNR as a Function of Range for Several Different Output Power Levels, Under Clear Dry Atmospheric Conditions (α = 3 dB/km).

2.0 TRANSMITTER

2.1 Transmitter Alternatives Considered

NMMW sources considered for use in the 220 GHz radar system were the optically pumped laser, the CW EIO, the IMPATT oscillator, and the pulsed EIO. The latter source was finally chosen, but this section will give some background on the basis for rejection of each of the others.

2.1.1 Optically Pumped Laser

The original request for proposal from NVL specified that the radar transmitter must be an optically pumped laser. In the initial Georgia Tech proposal, this laser transmitter requirement was addressed by proposing a CO_2 laser pumped $C^{13}H_3F$ cell with an expected output power of 8 kW peak and a PRF of 300 Hz. The CO_2 pump laser would weigh 700 kg and require primary power of 12 kW. Although this performance level has been improved upon in some instances, it is obvious that such a laser transmitter could not be scaled to a size such that it could be used in tactical applications without a major development effort. Based on this input from Georgia Tech, and apparently similar inputs from the other proposers, NVL decided to change the RFQ to specify an EIO transmitter. The optically pumped laser was therefore eliminated from consideration as a transmitter source for the NMMW radar because of its large size and weight, together with its relatively low PRF capability.

2.1.2 Continuous Wave Extended Interaction Oscillator

The original Georgia Tech proposal had as an optional transmitter approach the use of a CW EIO. This CW source was proposed instead of a pulsed source because it was considered likely that it would be much more amenable to frequency stabilization, thus providing a fully coherent system. The CW version of the EIO also has higher average output power, which would contribute to better radar performance.

Between the time that the original Georgia Tech proposal was submitted and the NVL RFP change was received, the CW EIO transmitter approach was examined more closely. As a result, it was decided that this transmitter would not work in the proposed configuration, for reasons to be discussed below. The CW transmitter used a polarization rotating duplexer (transmit-receive switch) which depended for its operation on the change in sense of circular polarization when reflected from a target. This duplexing method works well and has been used in optical systems. However, in the proposed application, it was realized that reflections from unmatched optical surfaces within the system would be large enough to saturate the receiver. Even if the surfaces could be matched so that reflectivities were only about 0.001 and FM modulation were employed to separate the target return from the internal backscatter, the reflected power would still over drive the receiver. For this reason, the CW EIO transmitter was abandoned in favor of the pulsed EIO. It should be noted that the pulsed system uses the same type of polarization duplexer as that originally proposed for the CW system, but minimizes

receiver over drive by also employing a quasi-optical transmit-receive switch. It is also expected that the receiver will recover from saturation due to a short transmitter pulse before useful radar returns are received.

A possible way around the receiver saturation problem occurring with a CW source is to use frequency modulation of the transmitter in such a way that energy received at some frequency corresponds to a given range. In this way, receiver saturation is avoided by using appropriate filters, since transmit and receive frequencies are never the same. Since saturation generally occurs in the IF amplifier and not the mixer, filters may be placed after the mixer to avoid IF saturation. Although CW radars have been built which use this method of receiver isolation, this FM-CW system was not considered for the NMMW radar because some difficulty was experienced with this approach during an earlier program conducted at Georgia Tech.

In summary, the CW EIO transmitter, although considered a viable approach for use in the NMMW radar, was rejected because of expected difficulties with receiver isolation.

2.1.3 Pulsed IMPATT

The pulsed IMPATT oscillator was also considered as a NMMW radar transmitter. Although capable of PRF's of several tens of kilohertz, these devices do not have enough power output capability at 220 GHz to perform effectively in the proposed radar system. Peak pulse powers of only 10 - 20 mW have been obtained. Furthermore, IMPATT's at these frequencies are generally unreliable because of the small size of the semiconductor chip. Also, it has not been possible to lock IMPATT devices at these

frequencies because their broadband noise output exceeds the bandwidth of the locking system. The IMPATT transmitter was therefore rejected on the basis of low output power, poor reliability, and difficulty in frequency stabilization.

2.1.4 Pulsed Extended Interaction Oscillator

The final alternative considered for the radar transmitter was the pulsed EIO. This source has good power and PRF capability, is of rugged construction, and has good possibilities for phase and/or injection locking. The short pulse output also provides a means of building an effective duplexer. This transmitter approach will be discussed in more detail in the sections that follow.

2.2 Description of Transmitter Subsystems

2.2.1 General Description

Figure 2-1 is a block diagram of the NMMW transmitter subsystem, and Table 2-I summarizes the transmitter specifications. Note that every frequency is referenced to the 97.5 MHz crystal reference oscillator, which is a source designed specifically by Hughes Aircraft to have a phase noise of better than -50 dBc/kHz throughout the entire spectrum of interest. This frequency represents a slight change from the 60 MHz source discussed at the design review because these high performance crystals are available only at frequencies near 100 MHz. Not shown in the figure is the fact that the same reference frequency is used to phase lock the Gunn oscillator which in turn serves as the receiver local oscillator.

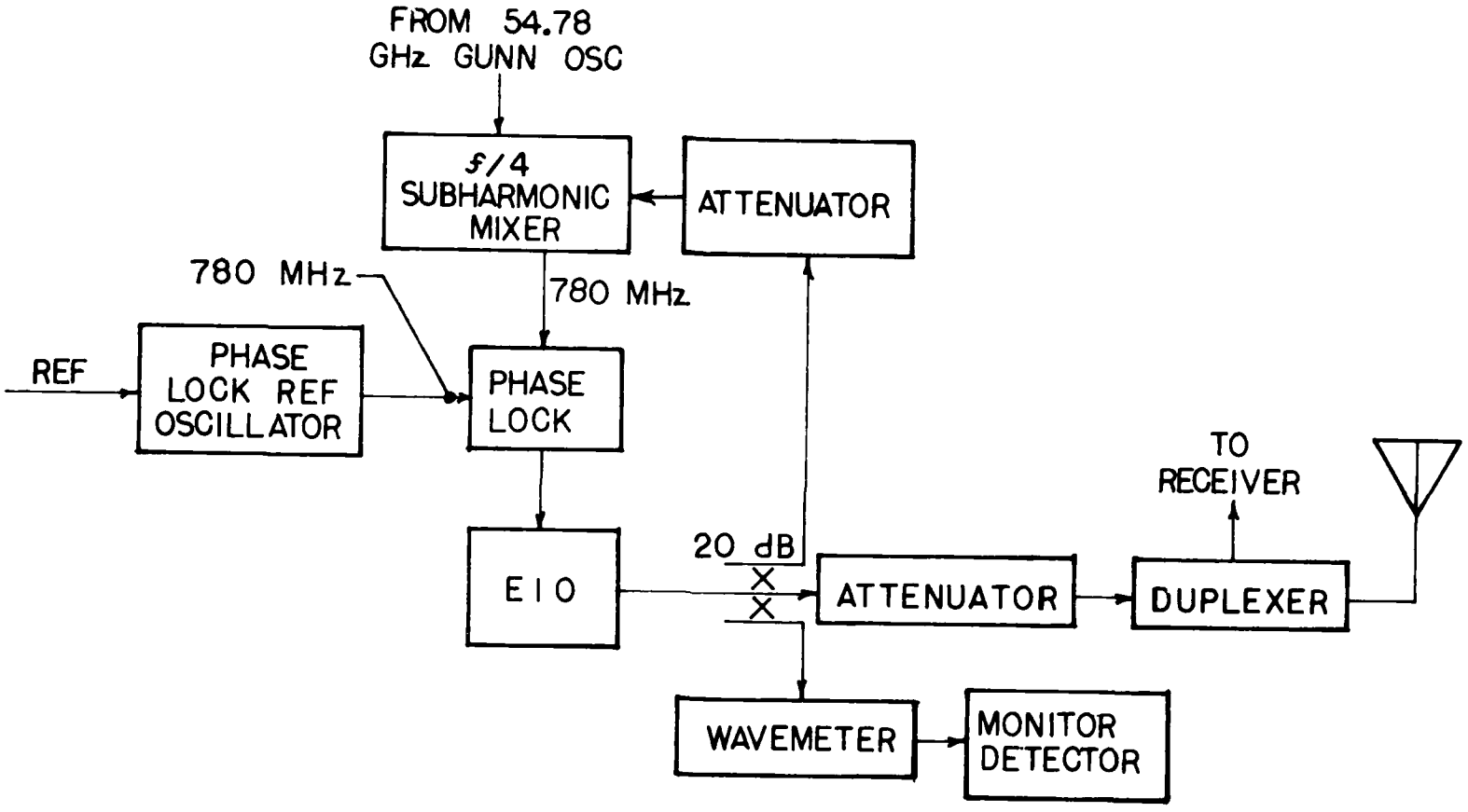

Figure 2-1. 220 GHz Radar Transmitter Block Diagram.

TABLE 2-I. TRANSMITTER SPECIFICATIONS

. FREQUENCY	219.96 GHz
. POWER OUTPUT	60 W PEAK
. PRF	5 - 25 kHz
. PULSE WIDTH	50 - 200 ns
. TUBE TYPE	VARIAN VKY-2429R EIO
. MAXIMUM DUTY FACTOR	0.005

The 97.5 MHz oscillator is used as a reference for the 780 MHz source, which is then used as a phase lock reference. This signal is combined with the 780 MHz phase lock intermediate frequency to generate a phase error signal for stabilization of the EIO. This IF results from mixing the 219.960 GHz EIO output with the fourth harmonic of the 54.795 GHz Gunn oscillator in the f/4 subharmonic mixer. Note that both of these frequencies have changed slightly from those presented at the design review because of the change in the crystal reference oscillator noted above. The EIO output is fed through an attenuator to the duplexer and from there to the antenna. The receiver, duplexer, and antenna will be discussed in later sections. Note that the attenuator in the EIO path will waste power, even when set for minimum attenuation. This component may be removed later, but is required for initial set-up of the duplexer to prevent damage to the receiver. The frequency and power of the EIO output are monitored by the wavemeter/monitor detector combination.

It must be noted that EIO's provided by Varian at 220 GHz are not well controlled regarding center frequency. The center frequency specification on the tube for this transmitter is 220 $\pm$ 10 GHz. If the tube will not oscillate within about 100 MHz of 220 GHz, it will be necessary to change the system frequencies, including both the crystal reference and local oscillator frequencies, to compensate. If the center frequency deviates from 220 GHz by more than 1 or 2 GHz, the Gunn oscillator will have to be returned to Hughes for retuning. It is necessary to order the Gunn at this time to assure prompt delivery and program continuity. Varian is studying methods of improving their manufacturing control over center frequencies.

2.2.2 Extended Interaction Oscillator Operation

It is of interest to briefly discuss the operation of the EIO, which is a high vacuum electron tube having a filament, cathode, anode, periodic structure, and collector. Figure 2-2 is a schematic diagram of this tube. Electrons emitted from the cathode are accelerated by the anode and focussed by the focus electrode and an external magnetic field into a very narrow beam. This beam passes through the resonator periodic structure and is modulated by it. The resulting electromagnetic energy is coupled out of the tube via a waveguide output. Some mechanical tuning capability is provided in lower frequency tubes by the tuning piston, but higher frequency tubes, including those operating at 220 GHz, are fix-tuned. The electron beam passes through the periodic structure and impinges on the collector, which carries almost all of the tube current, and is therefore generally cooled by either water or forced air. An advantage this tube configuration over many other tube types, including magnetrons in particular, is that the frequency determining electrode carries almost no current and is therefore only minimally subject to degradation caused by erosion and pitting due to impinging electrons. Only stray electrons are collected by the periodic structure in a well-focussed tube.

2.2.3 Modulator Operation

A schematic diagram of the modulator/EIO interface is shown in Figure 2-3. The EIO is operated as follows. The collector of this tube operates at ground potential. The periodic structure, from which the output is

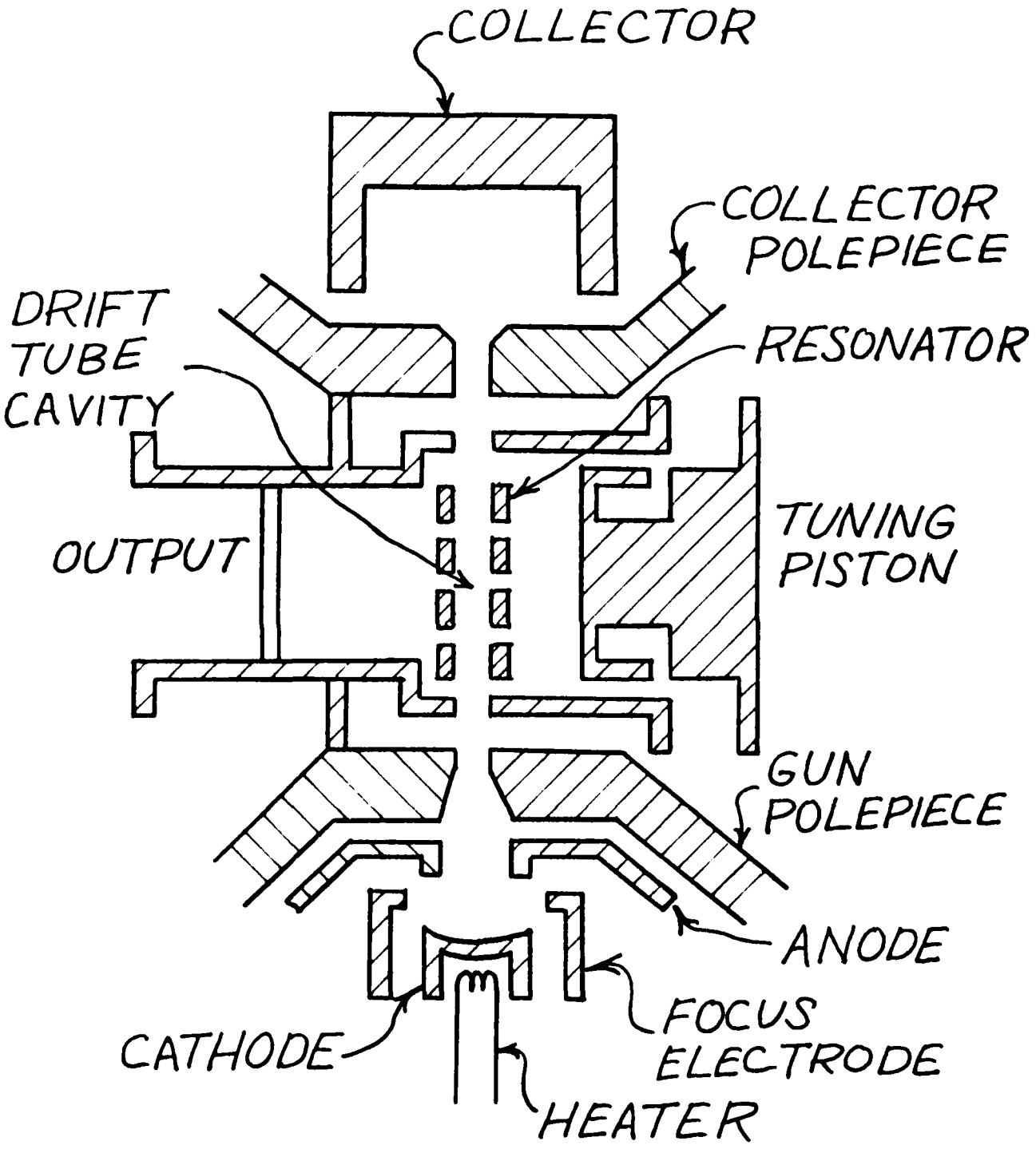

Figure 2-2. Schematic Diagram of Extended Interaction Oscillator.

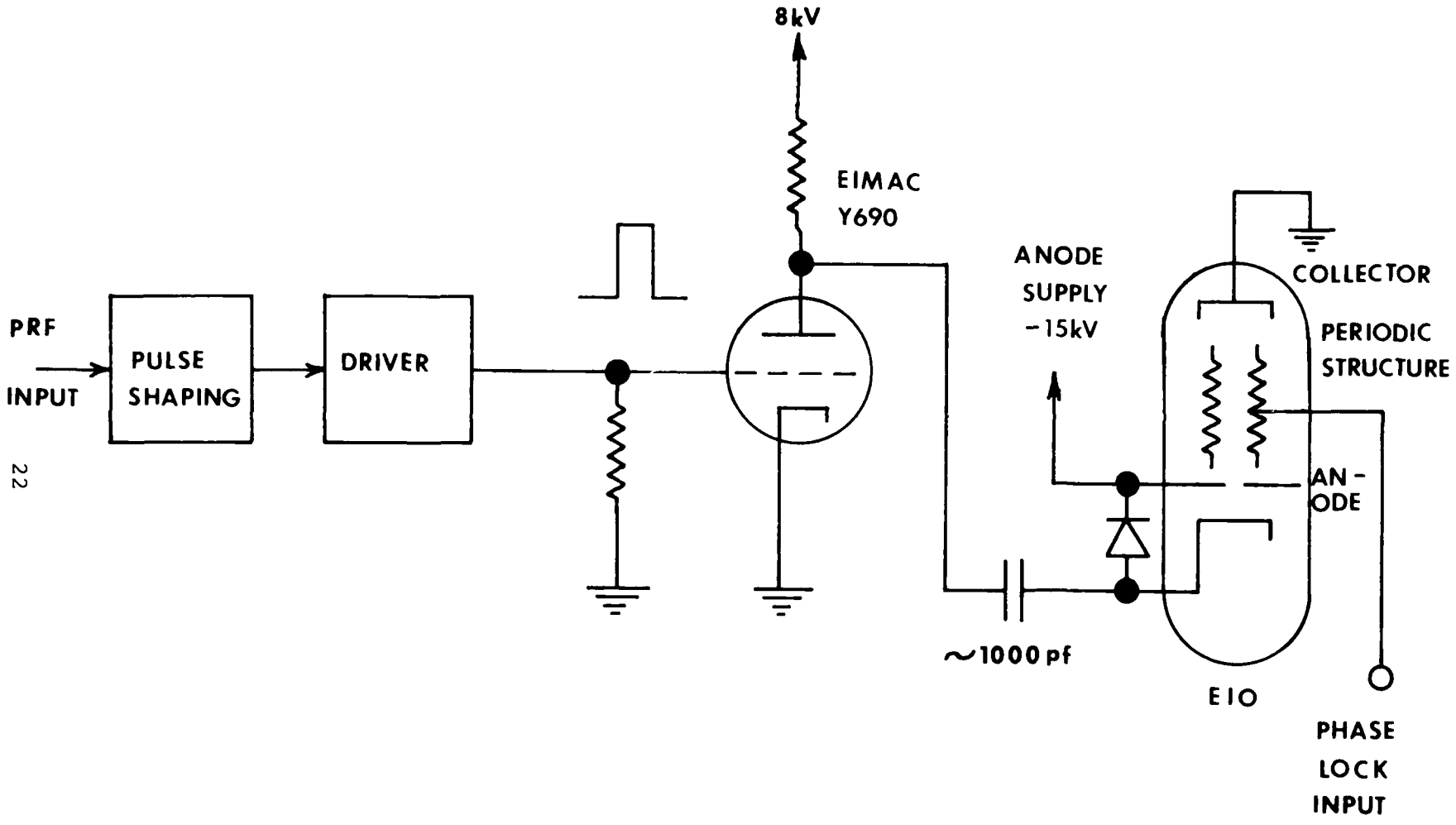

Figure 2-3. EIO Modulator Schematic Showing Interface with EIO.

taken, also operates near ground except for the effect of a phase lock correction voltage applied to it, which will normally be on the order of $\pm$ 100 volts. The anode is held at a negative potential of about -15 kV by a regulated power supply which is also coupled to the cathode by a diode or by an RF choke. The anode and cathode are at the same potential and the tube does not conduct. The tube is turned on by a negative 5.5 kV pulse applied to its cathode by the modulator through the coupling capacitor. This pulse is obtained by turning on the Y690 planar triode modulator tube in such a way that it is not saturated, so that its grid retains control over plate current and can therefore be used to correct for pulse droop and other deviations from flatness.

It is important that the EIO cathode drive pulse be maintained as flat as possible because the frequency output of the EIO is strongly dependent on the difference in voltage between the cathode and the periodic structure. Any voltage change appearing on the cathode must be compensated by a corresponding change appearing on the periodic structure, which must be furnished by the EIO phase lock circuitry. Since this circuitry will have limited speed and dynamic range, it is necessary to minimize changes between the cathode and periodic structure.

Compensation for pulse droop, ringing, and initial stray capacitance surge is accomplished in the modulator pulse shaping circuitry, shown schematically in Figure 2-4. A pulse of 10 ns or slightly longer length is applied to the input of a cascade of two 10-tap delay lines as shown. These delay lines have a delay of 10 ns/tap. The sum of the outputs of these circuits is then a single 200 ns pulse made up of 10 ns segments which are individually controllable in

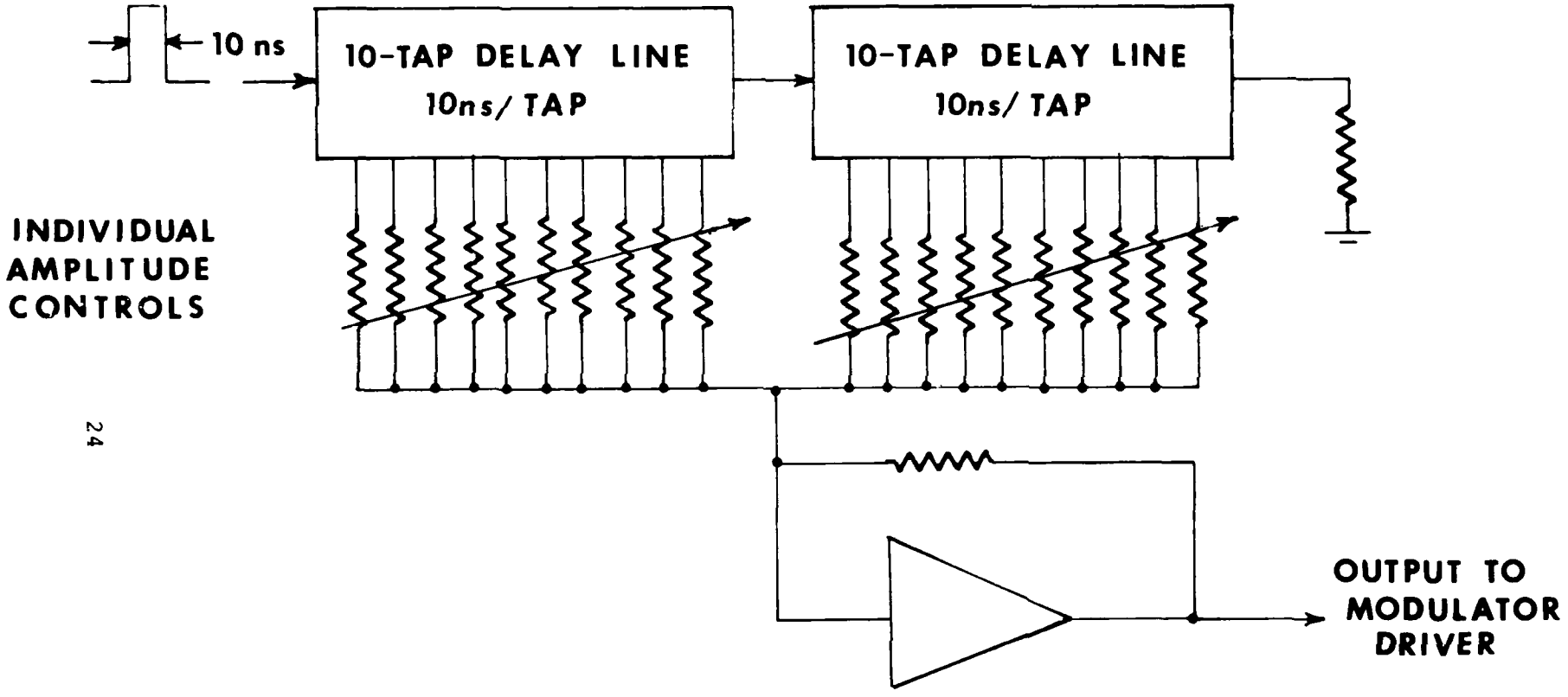

Figure 2-4. Modulator Pulse Shaping Circuitry.

amplitude by varying the size of the summing resistor in series with each output as shown in the figure. This arrangement may be used to provide an initial voltage spike to rapidly charge the EIO cathode stray capacitance to give fast RF pulse rise time. Also, the amplitude of each succeeding segment may be slightly increased to compensate for coupling capacitor discharge droop. Ripple or ringing on the RF pulse may also be corrected in this way. Modulator pulse width is varied by changing the total number of delay segments used to form the drive pulse. This type circuit has been used to generate an 8 kV pulse that is flat to within $\pm$ 15 V. Table 2-II summarizes the modulator specifications.

A brief analysis of modulator performance follows. In these calculations, general assumptions are made which may not be valid, such as a value for EIO capacitance and the fact that the modulator tube is saturated during turn-on. These calculations should therefore be considered as typical, and not strongly indicative of final modulator performance.

RF pulse rise and fall times are determined by the charge/discharge times of the EIO cathode stray capacitance. Figure 2-5 shows the shape of the cathode drive pulse. The turn-on time is a function of the fall time of the negative going leading edge of the pulse. This time constant is given by

$$t_f = R_f C_s = \frac{r_p R_L}{r_p + R_L} C_s , \qquad (2\text{-}1)$$

where r_p and R_L are plate and load impedances of the modulator tube, respectively, and $C_s \sim 50$ pf is the EIO cathode stray capacitance. As shown in the figure, the EIO

TABLE 2-II. MODULATOR SPECIFICATIONS

RF Rise & Fall Times	10 ns max
Pulse Width	50 - 200 ns, variable
PRF	5 kHz - 25 kHz, variable
Pulse Flatness	50 V Peak-to-Peak
Filament Power Supply	dc

NOTES:

1. Pulse width and PRF may be adjusted so as to give a maximum duty factor of 0.005, subject to the limitations given above.

2. A long pulse mode in which the pulse width could be extended to 500 ns with minimal circuit changes will be provided. This mode will be used to test locking techniques and will be subject to the 0.005 duty factor limitation.

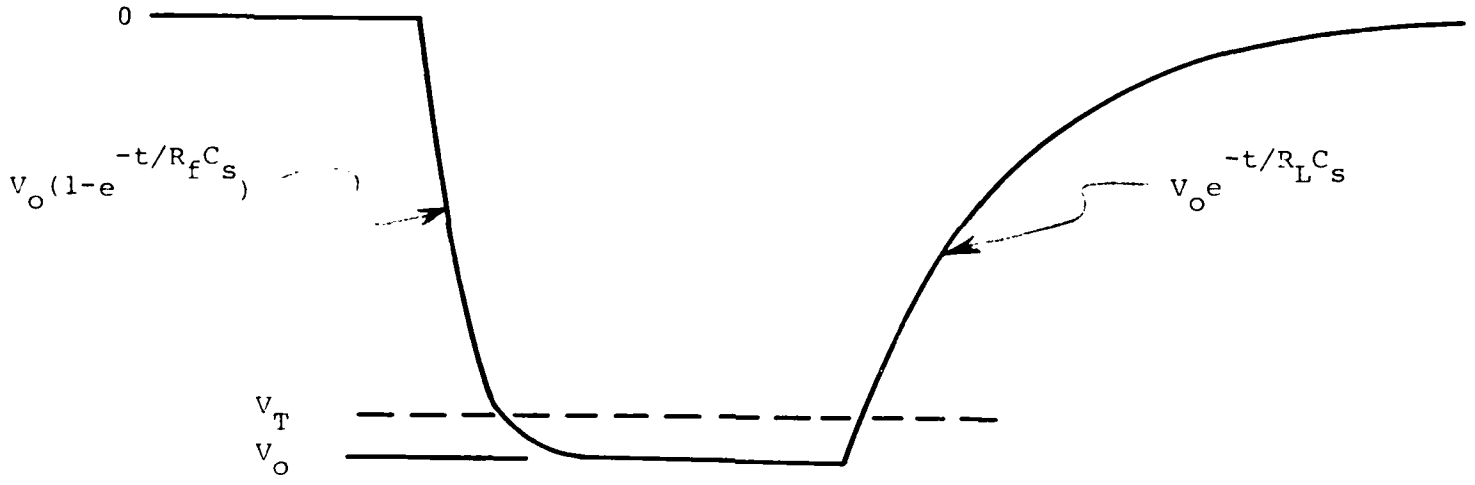

Figure 2-5. Idealized Shape of EIO Cathode Drive Pulse.

has a given threshold voltage above which it will not oscillate. Using the above time constant, it is easy to show that the threshold voltage V_T is reached in a time t_T given by

$$t_T = R_f C_s \ln \left(\frac{V_o}{V_o - V_T}\right) , \qquad (2\text{-}2)$$

where V_o is the final voltage value. Referring to the plate characteristic curves for the Y690 modulator tube, it is seen that the plate load resistance is about 150 Ω for the saturated condition. It is assumed that the tube is driven into saturation by the initial charging spike of the pulse shaper. In this case, the parallel combination of r_p and R_L is 130 Ω for R_L = 1000 Ω, and the turn-on time constant is (130 Ω) (50 pf) = 6.5 ns. If V_o = 5.5 kV and V_T = 5 kV, the time to reach threshold is then 15.6 ns. This time represents a delay between the time that the pulse is applied to the cathode of the EIO and that time at which the tube begins to oscillate. Of more interest is the time difference between the onset of oscillation and the time required for the cathode to reach a voltage that differs from the final cathode voltage by an amount that is within the dynamic range of the phase lock correction circuit. At this time, the phase lock will ideally begin to control the EIO frequency. If this voltage differs from the final voltage by 50 V, consistent with a $\pm$ 50 V dynamic range of the correction circuit, the time required for this voltage to be reached after initiation of the turn-on pulse is 30.6 ns, so that the time required for the phase lock to control the EIO frequency is 30.6 ns - 15.6 ns = 15.0 ns after onset of oscillation. Note that these numbers are idealized and do not allow any time for phase lock circuit propagation

times or other unaccountable delays. In any case, it can probably be stated from the above analysis that the rise time of RF oscillation is about 15 ns.

To calculate the fall time of oscillation, it is necessary to consider the trailing or rising edge of the modulator drive pulse shown in Figure 2-5. Since the modulator tube is turned off during rise time, the time constant is

$$t_r = R_L C_s , \tag{2-3}$$

and the time required for the EIO cathode voltage to again pass through threshold is

$$t_T = R_L C_s \ln \frac{V_o}{V_T} . \tag{2-4}$$

Using the parameters given above, this time is $t_T = 4.8$ ns, so that the RF oscillation fall time is about 5 ns. It thus appears that modulator pulse leading edge or fall time speed is likely to be more difficult to achieve than the trailing edge speed, contrary to some earlier predictions.

Modulator power dissipation is also of interest. It is easy to show that almost all of the modulator power is dissipated in the plate load resistor of the Y690 tube and in the tube itself. Assuming that the plate load is 1 k Ω and the tube conducts 6 amps during "on" time, the average power dissipation for a 200 ns pulse with a 5 kHz PRF is

$$P = (8 \text{ kV})(6 \text{ a})(200 \text{ ns})(5 \text{ kHz}) = 48 \text{ W}. \tag{2-5}$$

Based on the rise and fall time analysis given above, it is

possible that this power dissipation might be reduced even further by increasing the size of the plate load resistor, since the size of this resistor evidently has little effect on modulator performance. This type of decision must await further experimentation.

2.2.4 Phase Lock Subsystems

Although the phase locked Gunn oscillator is part of the receiver subsystem, it is appropriate to consider it at this point along with the transmitter phase lock. Figure 2-6 is a block diagram of this oscillator. A stable, low-noise crystal oscillator operating at a frequency near 100 MHz is used as a reference to phase lock a medium power transistor source at a frequency of 4-6 GHz. A harmonic of this source is mixed with the fundamental output of the Gunn oscillator to generate an IF equal in frequency to the crystal reference. This IF is compared to the reference in the phase detector to generate a phase error signal which is used to control the bias of the Gunn source, thus controlling its frequency. If the Gunn is considerably off frequency such that it is outside the capture range of the phase lock loop, an internally generated search/sweep signal is used to bring it within locking range.

Figure 2-7 is a block diagram of the EIO phase lock. This circuit was originally designed by P. S. Henry [2] of Bell Laboratories and features a frequency discriminator circuit which automatically pulls the frequency of the EIO within range of the relatively narrow band phase lock loop. This circuit is thought to be especially useful for locking a pulsed source because the phase lock portion will lose

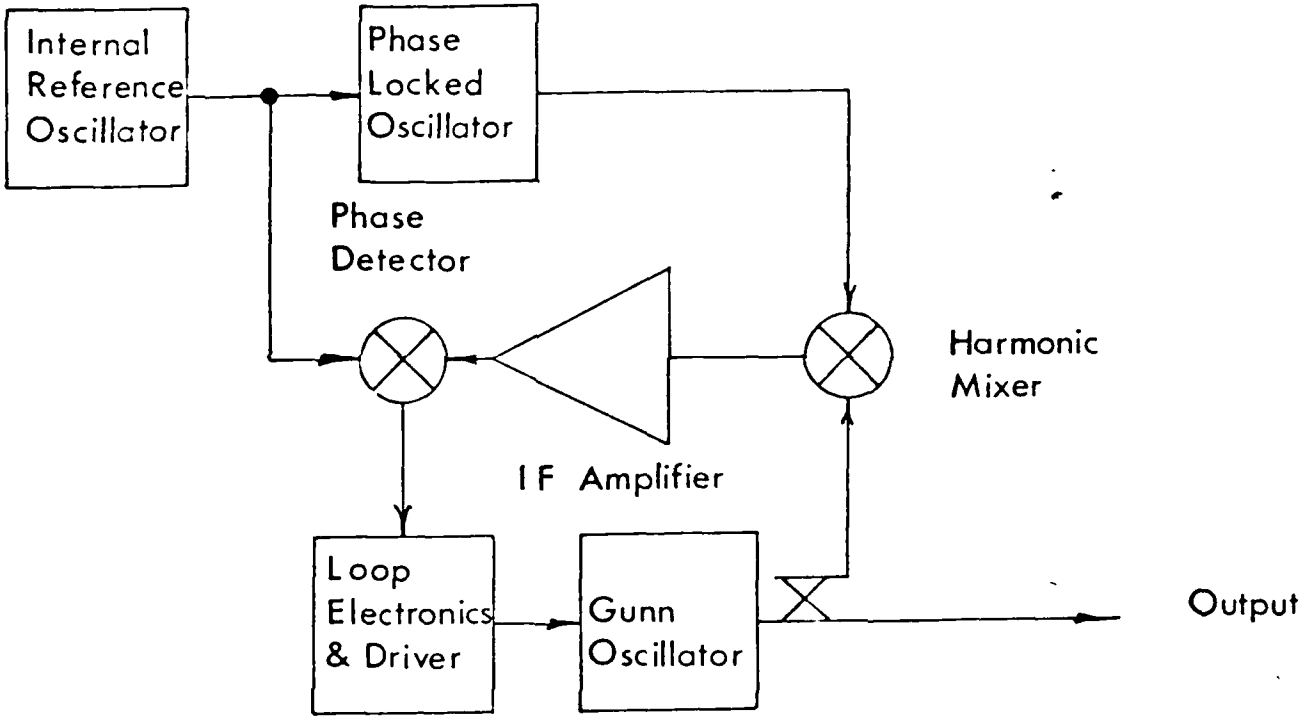

Figure 2-6. *Block Diagram of System Used to Phase Lock* Gunn Oscillators.

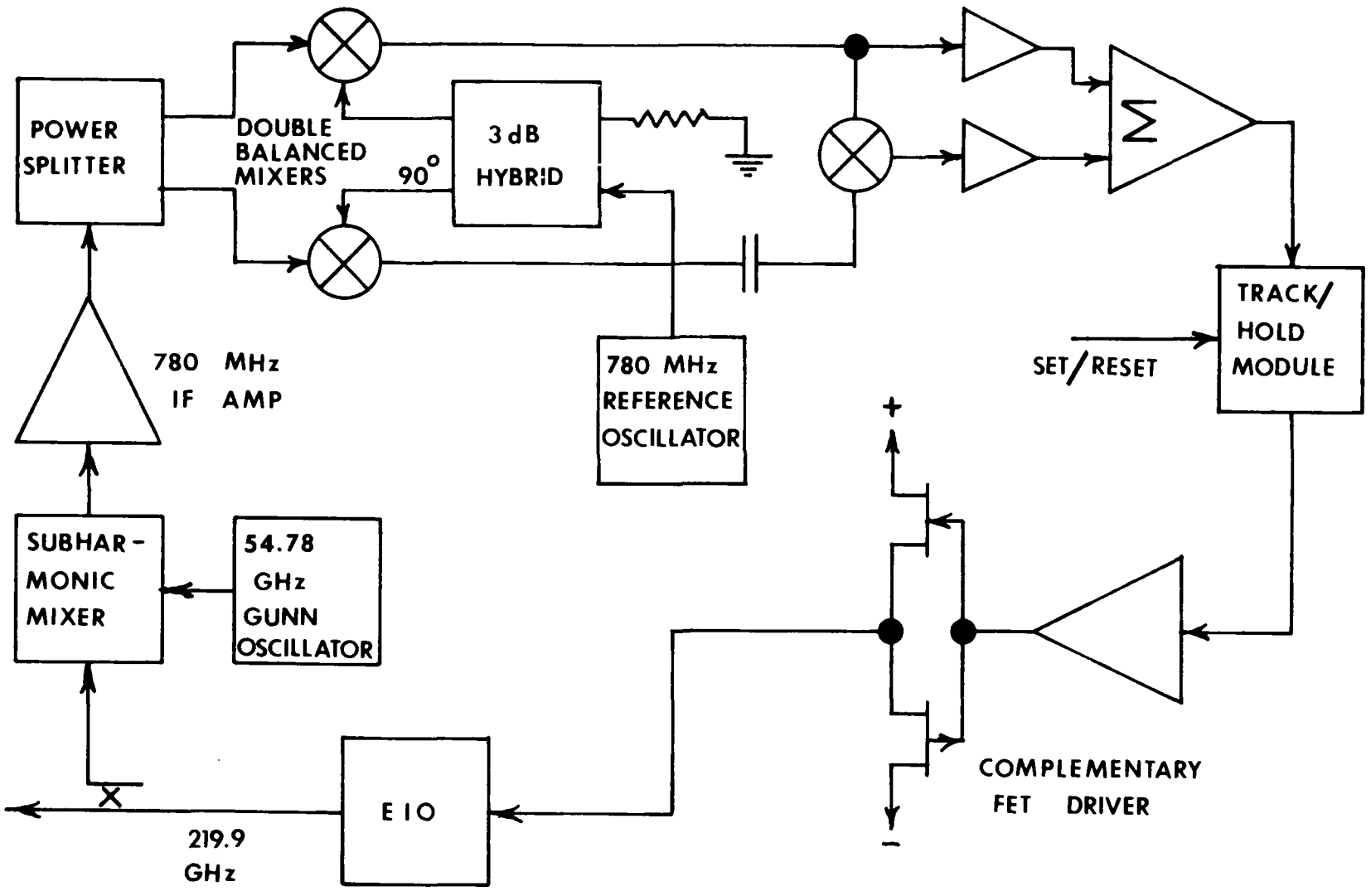

Figure 2-7. Block Diagram of EIO Phase Lock System.

control between pulses in the absence of signal, and will therefore likely begin oscillation at the start of the next pulse outside the range of the phase control loop. In this case the frequency control loop will act to change the tube frequency such that the phase loop regains control.

A more detailed treatment of the operation of this circuit follows. Part of the 219.9 GHz output of the EIO is picked off by a directional coupler and fed into an f/4 subharmonic mixer, where it is mixed with the fourth harmonic of the 54.8 GHz Gunn oscillator to give a 780 MHz IF. This IF power is split into two equal parts and compared to the output of a 780 MHz crystal-controlled reference oscillator in both in-phase and quadrature modes. For fully coherent operation, this oscillator will be phase locked to the 97.5 MHz oscillator which provides a reference signal for the entire system. If the EIO is locked, the output of the in-phase detector will be a dc correction voltage which changes little during the duration of the pulse. The output of the quadrature detector in this case is also a dc level which is blocked by the capacitor so that its output has no effect on the EIO frequency. The capacitor is chosen small enough to block the detected pulse output even though it is only 100-200 ns in length. Now assume that the EIO is unlocked. The outputs of both the in-phase and quadrature detectors will now be ac signals equal in frequency to the difference between the IF and the reference oscillator frequencies. Since the dc amplifiers driving the EIO periodic structure have limited bandwidth, the output of the in-phase detector will no longer influence the klystron frequency and the phase control loop is open. However, the outputs of both detectors will now be mixed in the multiplier, and its output will be a dc voltage that

varies with frequency error because of the presence of the capacitor. This correction voltage acts to pull the EIO within the frequency range of the phase lock loop, which recaptures the klystron, and disengages the frequency loop because the output of the quadrature detector is again a dc voltage blocked by the capacitor.

The correction voltages for frequency and phase are summed, passed through a track and hold module, and amplified to drive the EIO periodic structure. Since the pulsed output of the EIO is only a few hundred nanoseconds in length, the dc amplifiers used as drivers must have very wide bandwidths and fast slew rates to ensure that the EIO is locked before the end of its output pulse. The track/hold module is used to remember the correction voltage from the previous pulse to minimize the voltage change required from the dc driver amplifiers during a given pulse.

2.2.5 Possible Injection Locking Techniques

As stated in the preceding section, it will not be possible to phase lock the transmitter EIO during the leading and trailing edges of the modulator pulse because of the rapid changes in cathode voltage occurring during these times. The method of injection locking has some promise for solving this problem and for generally improving the quality of the lock over the entire EIO pulse. Briefly, this approach consists of feeding a stabilized signal into the output of the source to be locked so that it tends to oscillate in phase with this signal. However, there are some stringent requirements on the stability and power of this input, in addition to some difficulties involved in the actual injection, as will be discussed in succeeding paragraphs.

Injection locking of a 35 GHz Oki Laddertron, a pulsed tube similar to the EIO, has been done by Strauch [3], who found that an injection source power level of 17 mW was sufficient to lock the Laddertron in less than 1 μs. At lower injected power levels, correspondingly longer locking times were observed. An output power level of one watt at 220 GHz is available from either a CW EIO or a Carcinotron oscillator. If this power level is used to injection lock a 60 W EIO, the locking time should be only a few tens of nanoseconds or less. Note also that the simultaneous phase locking of the EIO should complement the injection locking and help to reduce locking times. It is expected that an injection locking source would itself be locked by a circuit essentially identical to that discussed in Section 2.2.4.

Figure 2-8 is a schematic of the approach considered best for injection locking. The locking source power is injected through a central obscuration and focussed into the transmitter EIO through its collimating lens. The transmitter power lost in this way is expected to be about 10-15%. A reduction of these losses could be effected by injecting the power off-axis, since the beam profile of the transmitter horn has a tapered (possible gaussian) shape, but this approach would probably cause assymmetry in the output beam, which would be undesirable. Off-axis injection will still be considered, however, if the existing contract is modified in the future to include injection locking.

Figure 2-9 shows another possible method of injecting power into the EIO, namely that of using a four-port circulator both for injection and for separating transmitter and receiver signals. This method was considered because TRG Division of Alpha Industries has offered to build a 220 GHz ferrite circulator for this program. However, the

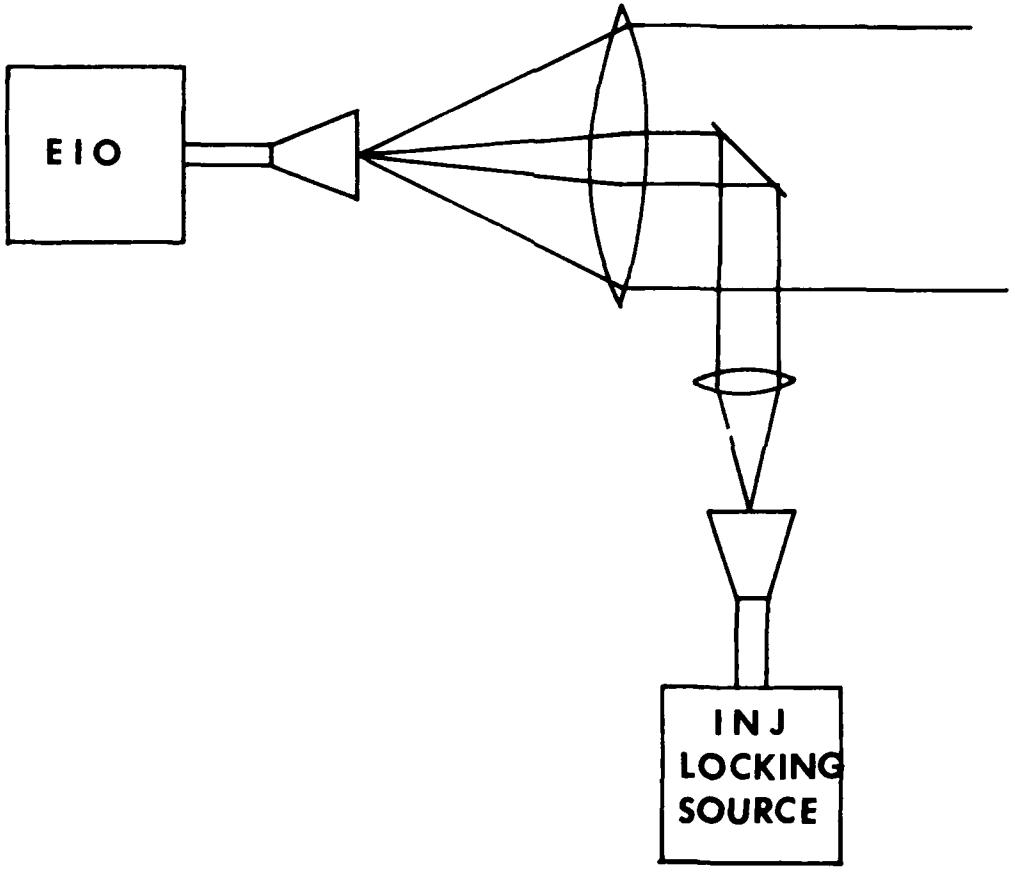

Figure 2-8. Schematic of Injection Locking through Central Obscuration.

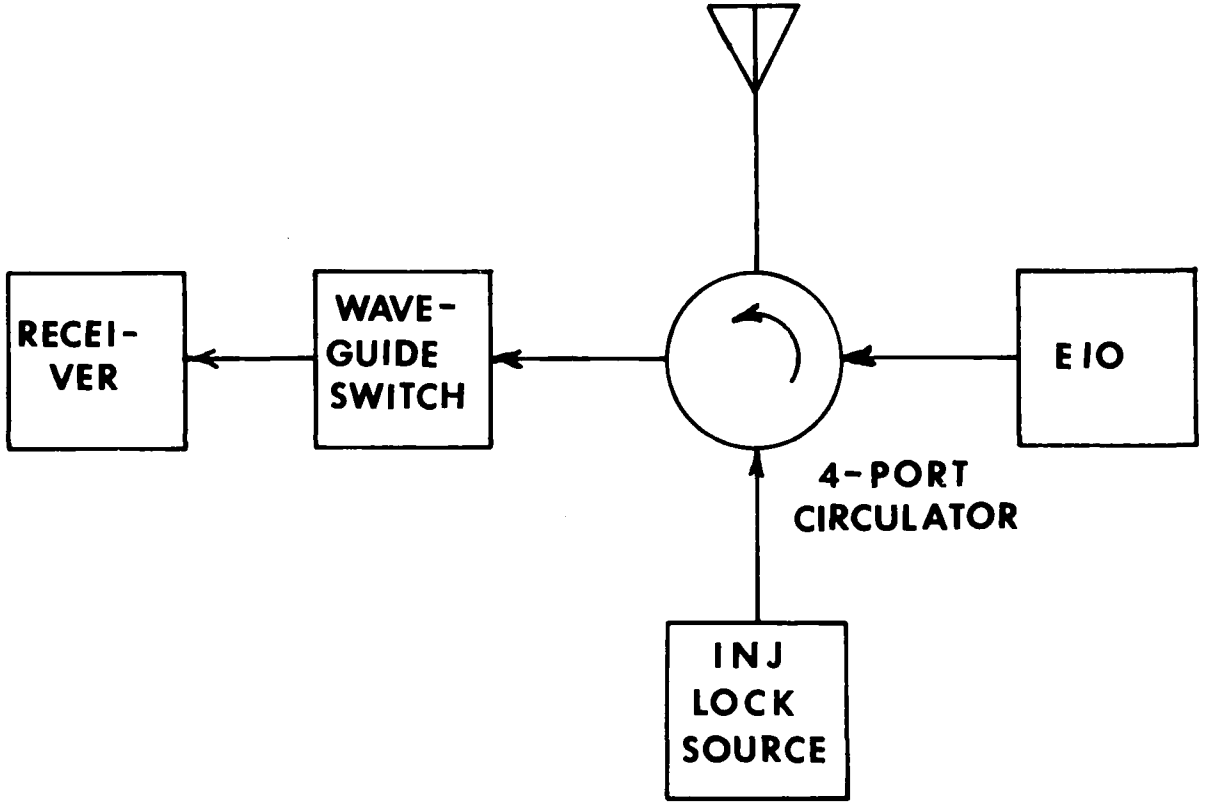

Figure 2-9. Injection Locking with a Four-Port Ferrite Circulator.

quasi-optical injection scheme is still considered best because the circulator has a 3 dB loss between adjacent ports and only has 15 dB isolation between non-adjacent ports.

At the present time, Georgia Tech has no charter to include injection locking in the system to be delivered to NVL. At the design review it was decided that addition of injection locking to the proposed system should await the results of a similar effort being carried out by Georgia Tech for U. S. Army MICOM, which is scheduled for completion early in 1980. The techniques learned in injection locking the MICOM source should be directly applicable to the NVL system.

3.0 RECEIVER

3.1 Receiver Description

The overall receiver system requires a down converter using a local oscillator that is phase locked to a baseline reference crystal oscillator. This is the same reference that is used to ultimately lock the transmitter during its operation. The local oscillator is monitored using frequency monitoring components to insure proper operation of the receiver. The intermediate frequency (780 MHz) is generated by the down converter when the returned power from the target mixes with the local oscillator. This is then amplified using a linear amplifier to preserve the phase information. This amplifier can be replaced by a logarithmic amplifier for non-coherent operation. The amplified signal (IF) is then detected using a second mixer with a phase locked 780 MHz baseline reference to produce a video output signal. This is then fed to an output monitoring device such as an oscilloscope.

3.2 Approaches Considered

Three basic approaches were considered for this 220 GHz receiver system. The first approach uses a mixer which operates with a local oscillator (LO) that is close to the signal frequency. The second uses a mixer which operates with a local oscillator at about half the signal frequency. The third uses a mixer that is pumped with a local oscillator at about one fourth the signal frequency of 220 GHz.

The first approach would require expensive waveguide components plus the development of an LO injection device or balanced mixer and a phase locked 220 GHz local oscillator. Some of these waveguide components, the LO injection device and the mixer would have to be duplicated in parts of the phase lock portion of the transmitter. The local oscillator would consist of a klystron along with its associated bulky power supply and cooling equipment. This klystron would be phase locked and drive a solid state doubler. This system would have a good noise figure but the large initial capital outlay in components and the required eventual replacement of klystrons makes the cost of this system very high when compared to the others described later in this report.

The second approach would involve the development of a 220 GHz subharmonically pumped balanced mixer which is pumped at one half the signal frequency. A 55 GHz injection locked Gunn could be doubled to provide 20 m W of LO power at 110 GHz. Subharmonic mixers would be used for both the phase lock mixer and the receiver mixer. Mixers of this type which operate at 183 GHz have already been built successfully here at Georgia Tech [4], and have shown state-of-the-art noise figures at that frequency. This design is easily scaled for use at 220 GHz.

The third approach which uses a 55 GHz local oscillator has several advantages over the two previously discussed and is therefore chosen as the primary approach. The main consideration for this choice is the large reduction in the cost of waveguide components and the availability of relatively inexpensive phase locked local oscillators. These advantages are obtained with negligible degradation in system noise figure. The expected noise figures for all three systems are shown in Table 3-I.

TABLE 3-I

APPROACH	ESTIMATED SYSTEM NOISE FIGURE (DSB)
Fundamental	12 dB
Subharmonic (X2)	11 dB
Subharmonic (X4)	12 dB

These numbers include a 3 dB contribution due to RF losses prior to the receiver and a 2 dB IF amplifier noise contribution.

3.3 Detailed Discussion

A subharmonic mixer is a mixer that is pumped by a local oscillator (LO) that is an integral submultiple of the signal frequency, neglecting the offset of the intermediate frequency (IF). Specifically, for the types of mixers developed at EES, the submultiples are even, so that the local oscillator frequency may be one-half, one-fourth, or possibly as low as one-eighth of the signal frequency. These mixers should not be confused with harmonic mixers, which are also pumped at submultiples of the signal frequency. This latter type of mixer is inherently noisy because of the comparatively high power dissipated in the mixer diode. The advantages of the subharmonic mixer with regard to local oscillator source requirements are obvious, but other advantages, especially the low noise performance, will be discussed later.

A subharmonic mixer with a frequency range of 183 $\pm$ 10 GHz has recently been designed, built, and tested at EES. This mixer uses an antiparallel diode pair and represents a significant advance in the state-of-the-art of subharmonic mixer development above 140 GHz. An IF bandwidth of 0.75 to 10 GHz was achieved with a double sideband noise figure of 5.0 to 8.5 dB, depending on the IF, while being pumped with an LO at 91.65 GHz.

A subharmonic mixer is designed by first modeling the device at a lower frequency, for example 6.8 GHz was used as the signal frequency for the EES design. At this frequency, the quartz stripline and other critical components can be more easily optimized. The design is then scaled downward in size by a factor of 26.9 to arrive at the design for 183 GHz. A design for the 183 GHz mixer using $f_s/2$ (f_s = signal frequency) pumping has been implemented with the results given above. A model for $f_s/4$ was also built and tested, and an $f_s/4$ subharmonic mixer for use at 183 GHz has been assembled and is currently being evaluated. The results of measurements on the $f_s/4$ model will be discussed later.

Some of the advantages of this type of mixer are:

- The local oscillator (LO) operates at 1/2 or 1/4 of the signal frequency of interest.
- Double sideband noise figures of 5 dB at 183 GHz have been achieved. A performance level of 7 dB is projected for a mixer designed to operate at 220 GHz.
- The mixer uses both waveguide and suspended quartz stripline filters to achieve low losses.
- Antiparallel mounted Schottky barrier diodes are located directly in the waveguide where the signal and local oscillator power mix. This arrangement requires no dc bias.

- Very wide RF and IF bandwidths are achieved providing an instantaneous bandwidth of about ± 5% of the signal frequency and an IF bandwidth of 5% of the signal frequency. For example, a 183 GHz mixer fabricated for NASA covers the range between 173 to 193 GHz with an IF between 0.5 and 10 GHz.

- Schottky barrier diodes are currently available with low resistance and low capacitance that have cut-off frequencies in excess of 3000 GHz.

- Design is easily scaled for other signal frequencies.

The chief advantage of using this type of mixer is that the LO frequency is only one-half or one-fourth of the signal frequency which eases LO requirements. This approach allows the use of relatively inexpensive and/or solid state local oscillators thus doing away with bulky klystron power supplies and coolers and decreasing replacement costs for the high cost and short lifetime klystrons.

The 183 GHz subharmonic mixers (X2 and X4) were both initially modeled at a signal frequency of 6.8 GHz to optimize the suspended substrate circuits used to inject the local oscillator frequencies and extract the IF frequencies. A diagram of the fourth harmonic mixer is shown in Figure 3-1. The diodes are mounted in an antiparallel fashion in the waveguide itself. A linear taper is used to reduce the signal waveguide height to facilitate RF matching. A variable backshort is used for tuning purposes. This backshort is located in the half-height portion of the waveguide and helps match the non resistive components in the RF impedance of the diodes. The LO filter is a low pass filter which is photolithographically etched on a 0.0025 inch thick quartz substrate that has been sputter-plated with a Cr-Au metallization on one side. This filter

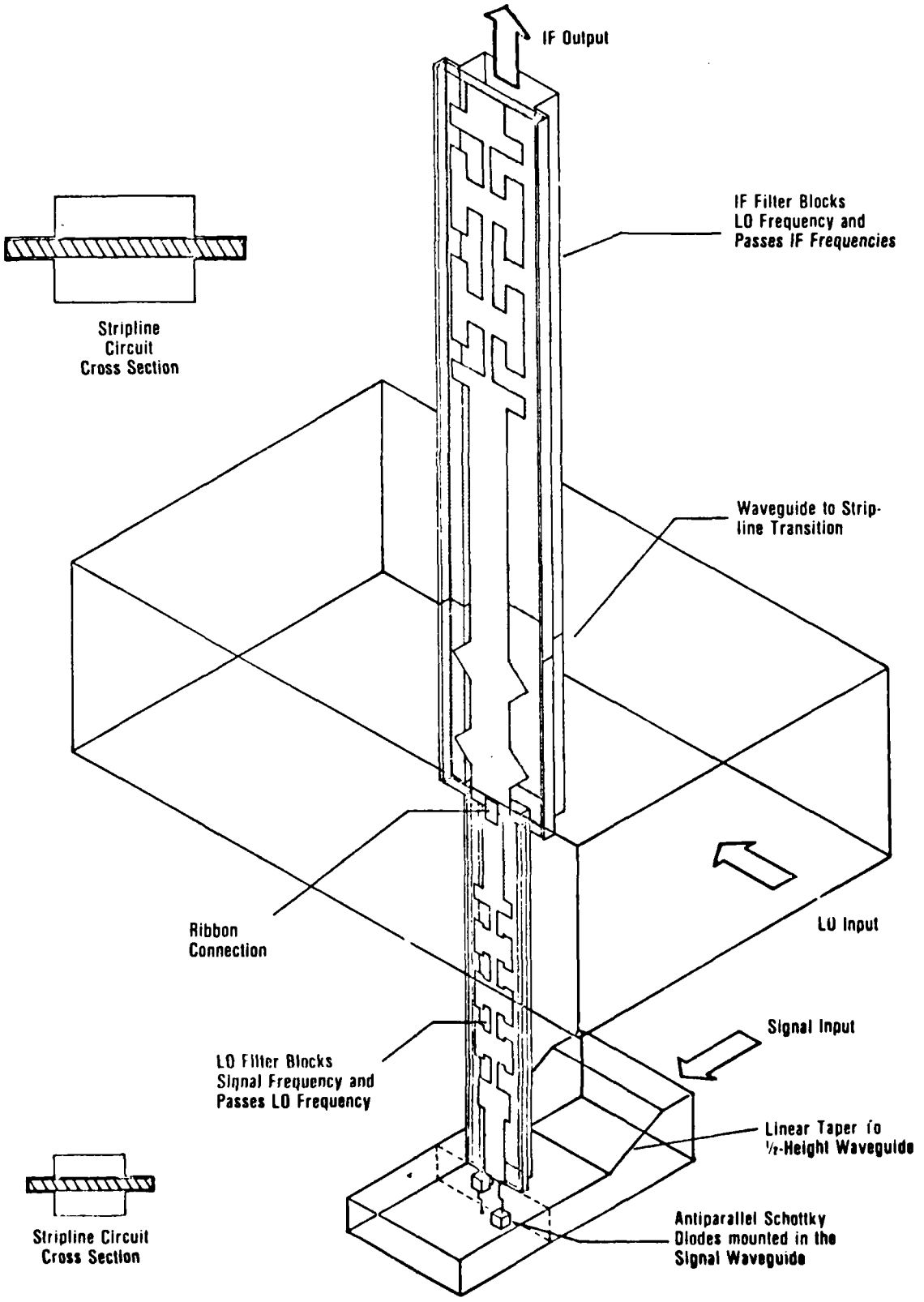

Figure 3-1. Fourth Harmonic Mixer Layout

performs the following functions: it blocks the 220 GHz signal from leaking out of the diode circuit; it matches the diode circuit to the signal power; it passes the LO frequency ($\sim$ 55 GHz in this case); it prevents the generation of X2 mixing components thus decreasing the noise figure and the conversion loss; and it passes the IF to the IF filter portion of the circuit above it. The use of two circuits eases fabrication and handling problems and improves circuit performance. The larger channel is used for the IF filter because only lower frequencies are present in this portion of the mixer. A gold ribbon connection is made to join the two circuits. The waveguide transition is the dual diamond structure located in the LO waveguide parallel to the E-plane of the LO power. This waveguide is also terminated with a variable backshort for tuning purposes. The LO power is launched onto the suspended substrate circuit in both directions (to the diodes and to the IF filter) with this transition. The IF filter is a similar low pass filter etched on a 0.005 inch thick quartz substrate which diplexes the IF and LO frequencies such that the LO is blocked by the filter and reflected in phase to the power that is sent directly to the diodes. The IF passes through this filter to the IF amplifier through an SMA connector joined to the substrate by a small ribbon connection. These filter functions are summarized in Figure 3-2. The actual results obtained with the model circuits are shown in Figures 3-3, 3-4, 3-5 and 3-6.

The suspended substrate configuration allows the use of the low loss transmission medium for injection of the LO since air is the major portion of this transmission medium. No losses are incurred on the signal due to the use of this technique other than the waveguide losses present since no

Filter	Scaled f_{cs}	Actual f_c	Insertion Loss $IL_{Sig.}$	IL_{LO}	Insertion Loss IL_{2XLO}	IL_{IF}
IF	0.9 GHz	29 GHz	——	39dB	——	0.1
LO	2.8 GHz	90 GHz	50dB	0.1dB	30dB	0.1

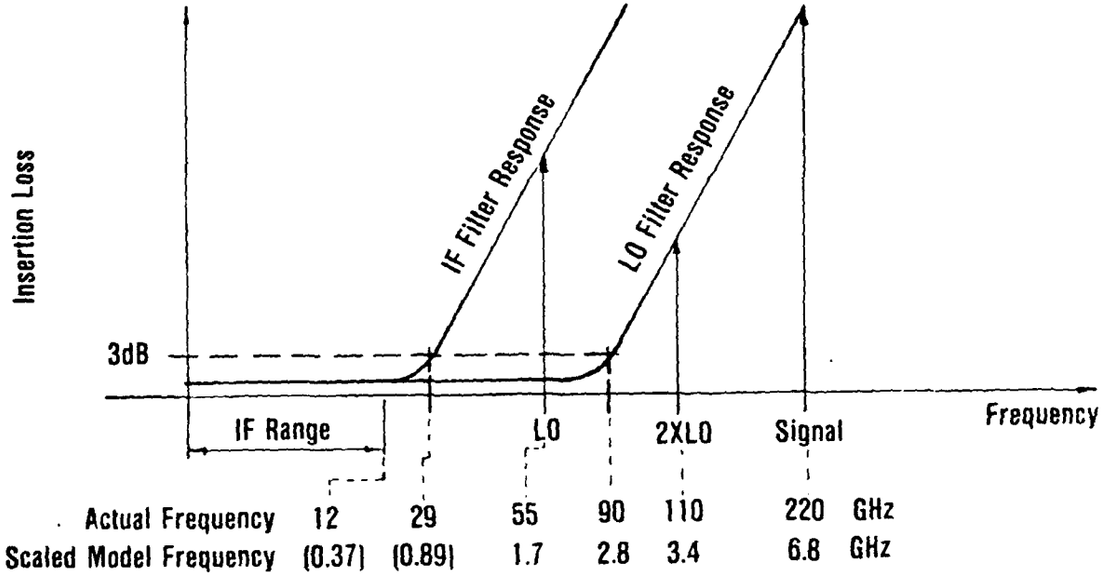

Figure 3-2. Filter Parameters and Data.

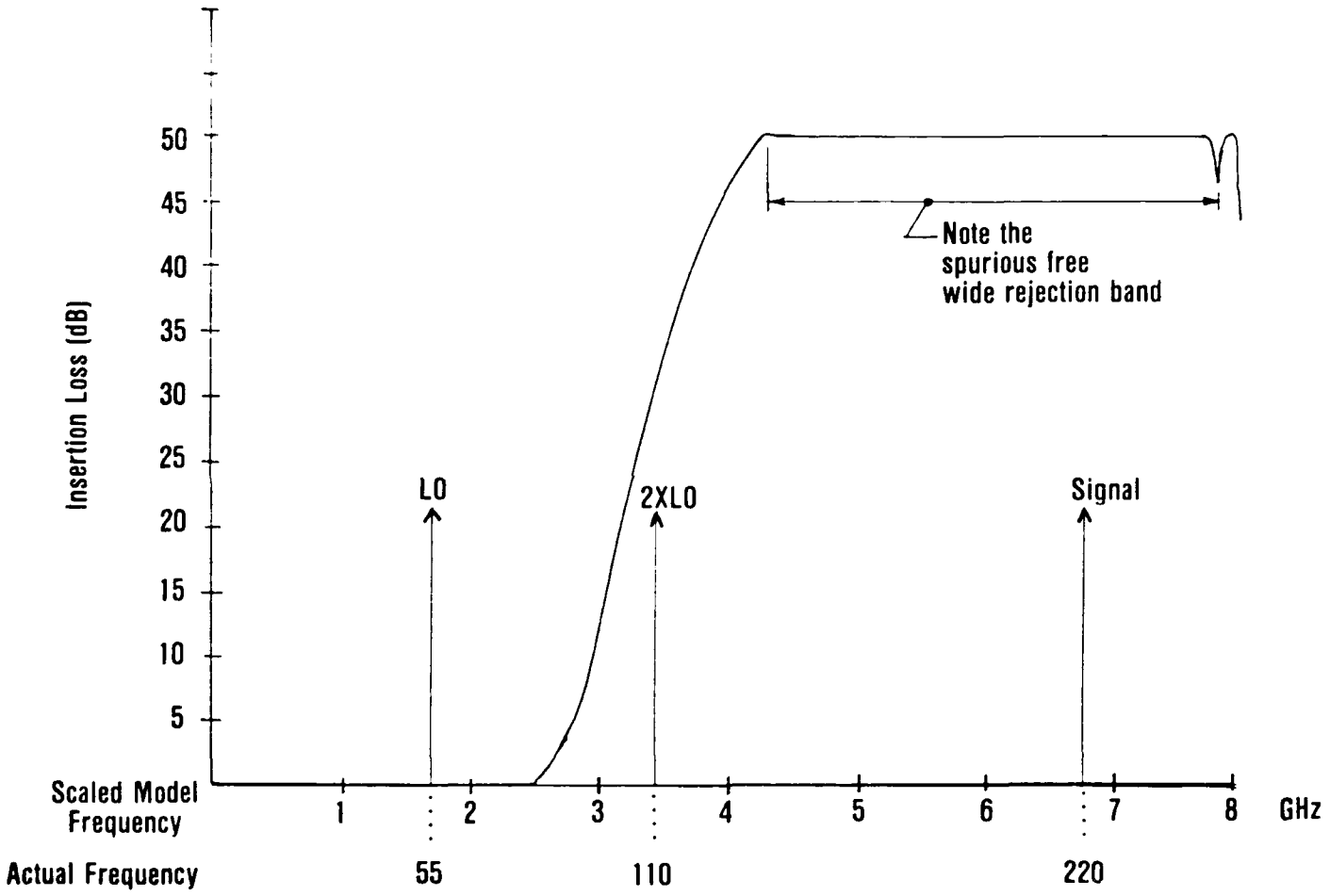

Figure 3-3. Measured Insertion Loss of the LO Filter for the Fourth Harmonic Mixer Model.

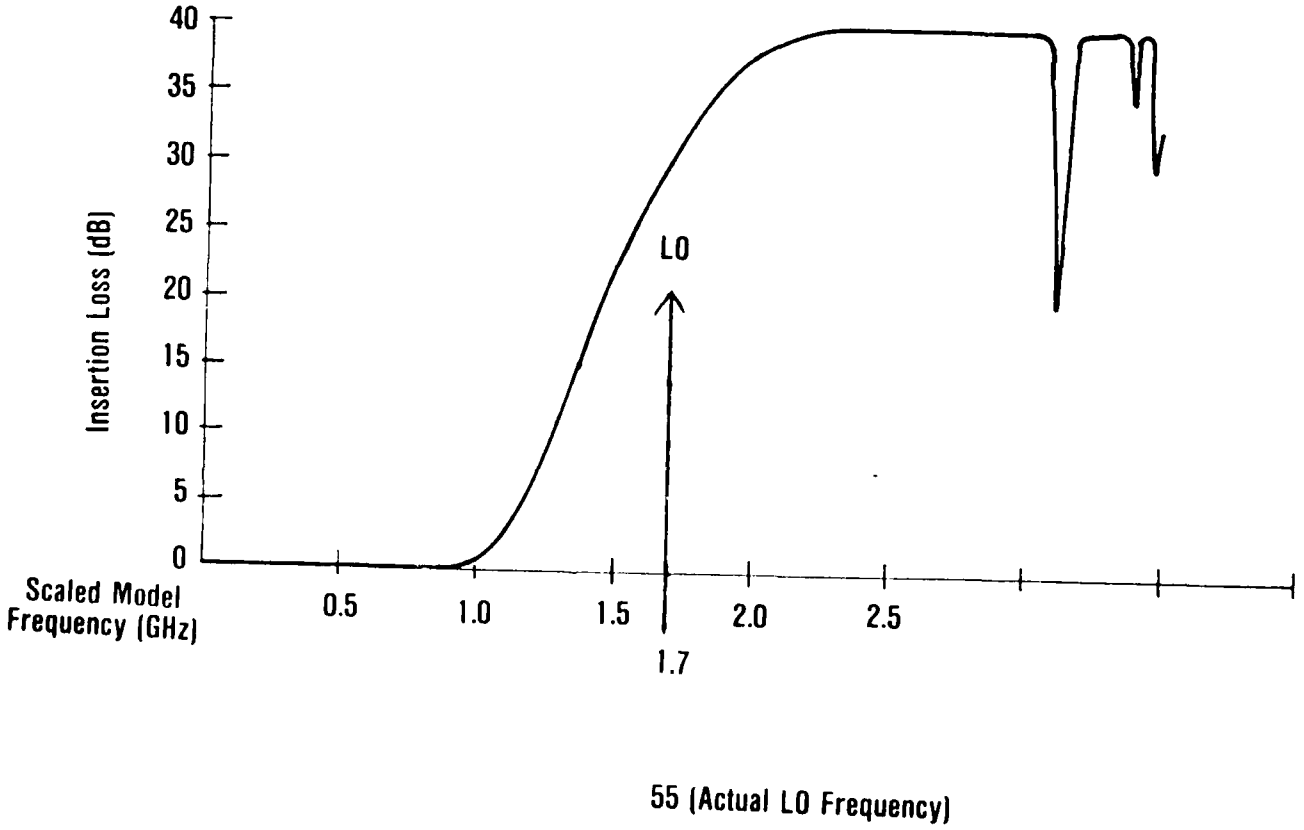

Figure 3-4. Measured Insertion Loss of the Scaled Model IF Filter.

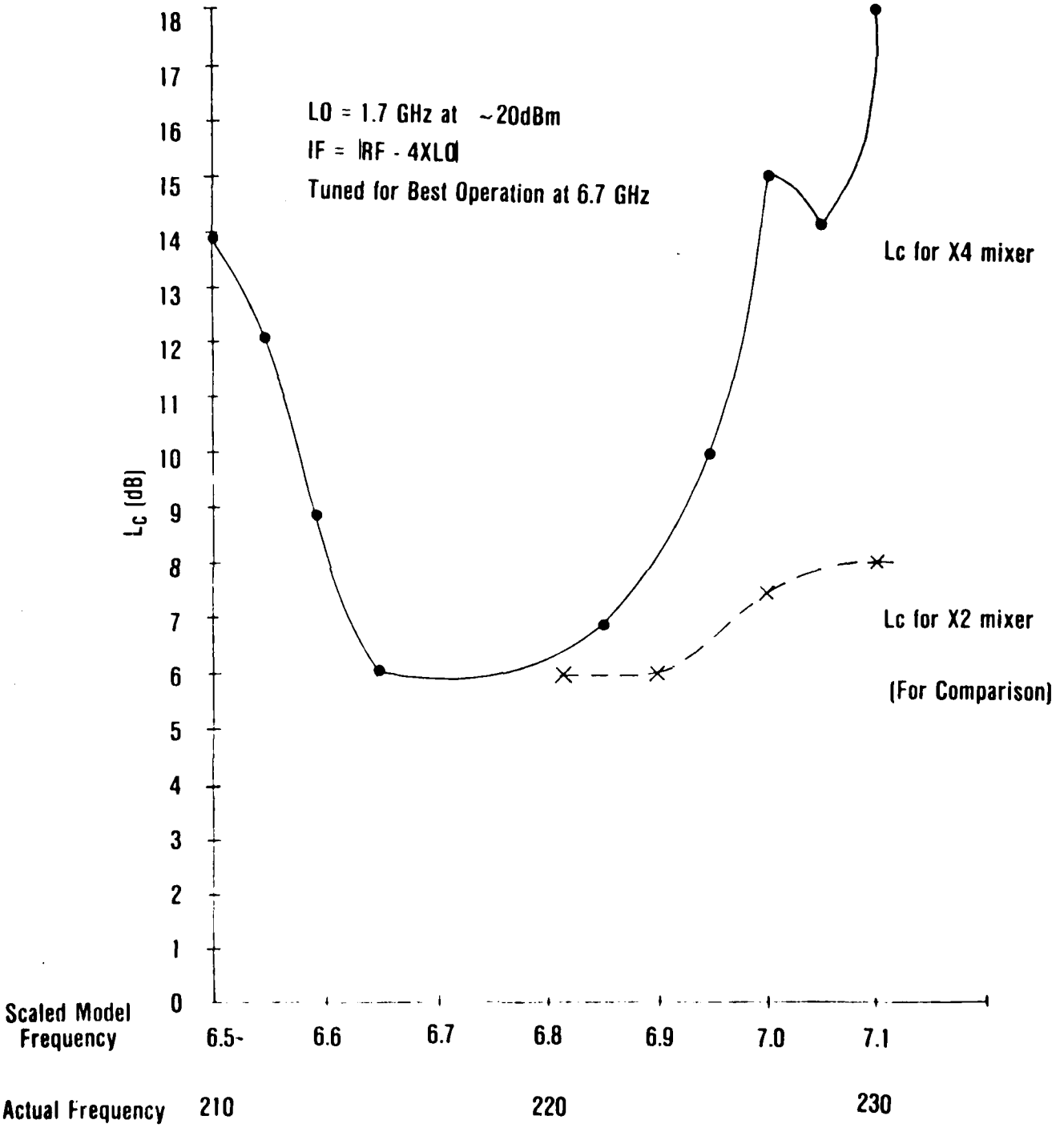

Figure 3-5. X4 Scaled Model Results: Conversion Loss vs. Frequency.

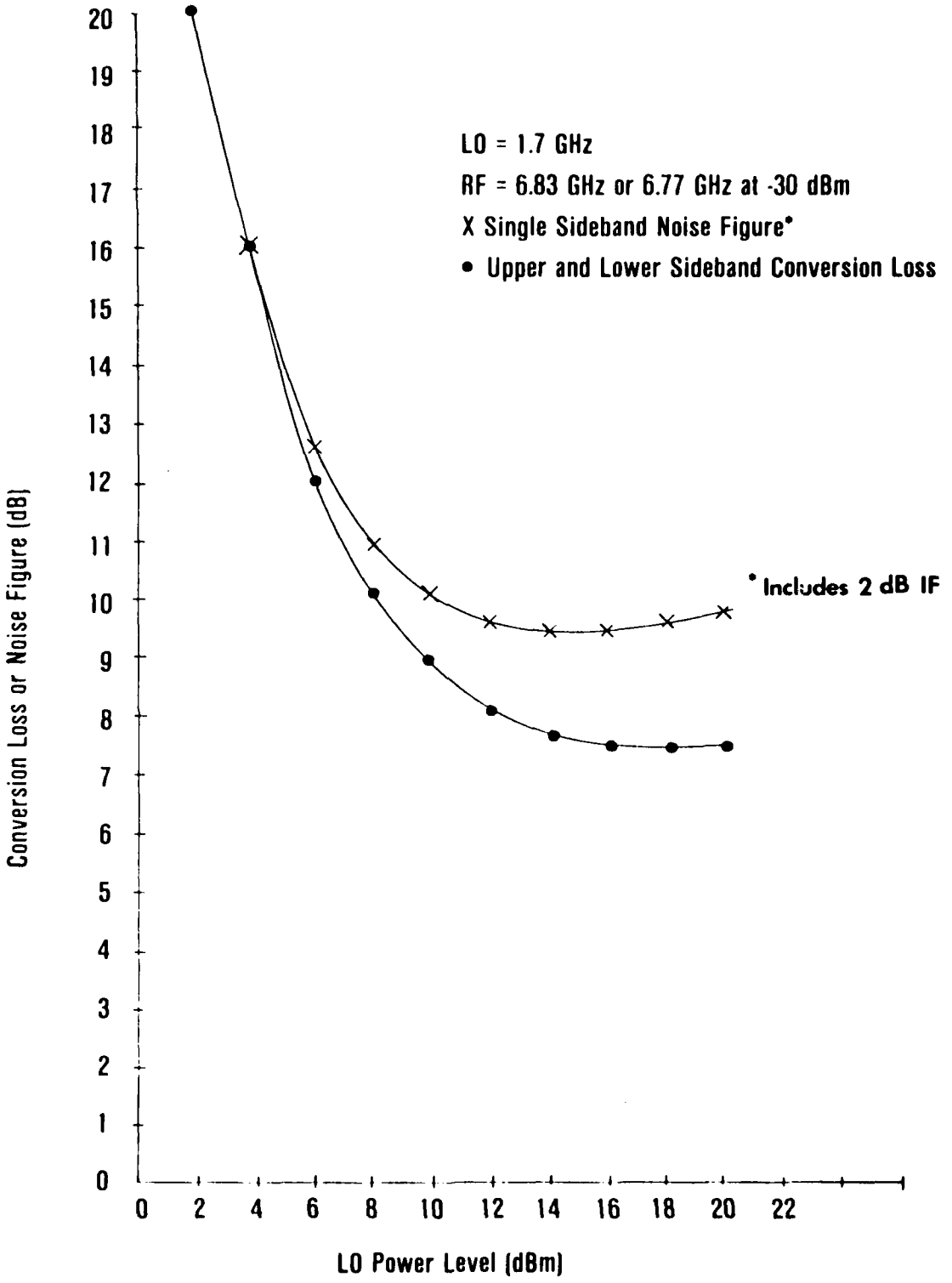

Figure 3-6. X4 Model Mixer Results: Conversion Loss and Noise Figure vs. LO Power.

signal power is transmitted through the stripline. It also allows the use of broadband low pass filters thus cutting down on the degree of tolerances normally required on high frequency bandpass LO injection techniques.

The diodes are located in the waveguide itself. One diode chip which contains a large array of 1.5 μm diameter Schottky diodes and one whisker are soldered onto the end of the substrate. Another diode and whisker are mounted on two separate posts about 0.032" in diameter. These posts are then press fitted into the other side of the mixer body from the bottom as shown in Figure 3-1 and contacted individually using a differential micrometer to push the pins in to make the ohmic contact to the diodes.

The 183 GHz version of this type mixer performed as the results of the scaling techniques had predicted. A 5 dB mixer noise figure was achieved at 183 GHz using the X2 mixer. The model predicted a 4 dB noise figure. The X4 model mixer predicts a 5 dB DSB mixer noise figure which implies that a 7 dB mixer noise figure can be achieved at 220 GHz. These results are given in Table 3-II showing achieved and predicted results obtained at Georgia Tech with these mixers.

The results of this portion of the study show that a highly sensitive, solid state, 220 GHz phase locked receiver is feasible and will be implemented under this contract using a fourth harmonic 220 Ghz balanced mixer. This receiver is shown in detail in Figure 3-7. A similar balanced mixer is also provided for the phase lock portion of the system.

TABLE 3-II. EXPECTED PERFORMANCE

- 7 dB DSB noise figure for mixer
  - Model measurements
  - 183 GHz X2 subharmonic mixer performance
  - Hot/cold load Y-factor measurement
  - 183 GHz X4 mixer soon to be tested
- Highly reliable
  - 183 GHz X2 subharmonic mixer flew at 60,000 feet

DEVICE	NOISE FIGURE (DSB)
X2 Model Mixer	4 dB
X2 183 GHz Mixer	5 dB
X4 Model Mixer	5 dB
X4 220 GHz Mixer	7 dB (projected)

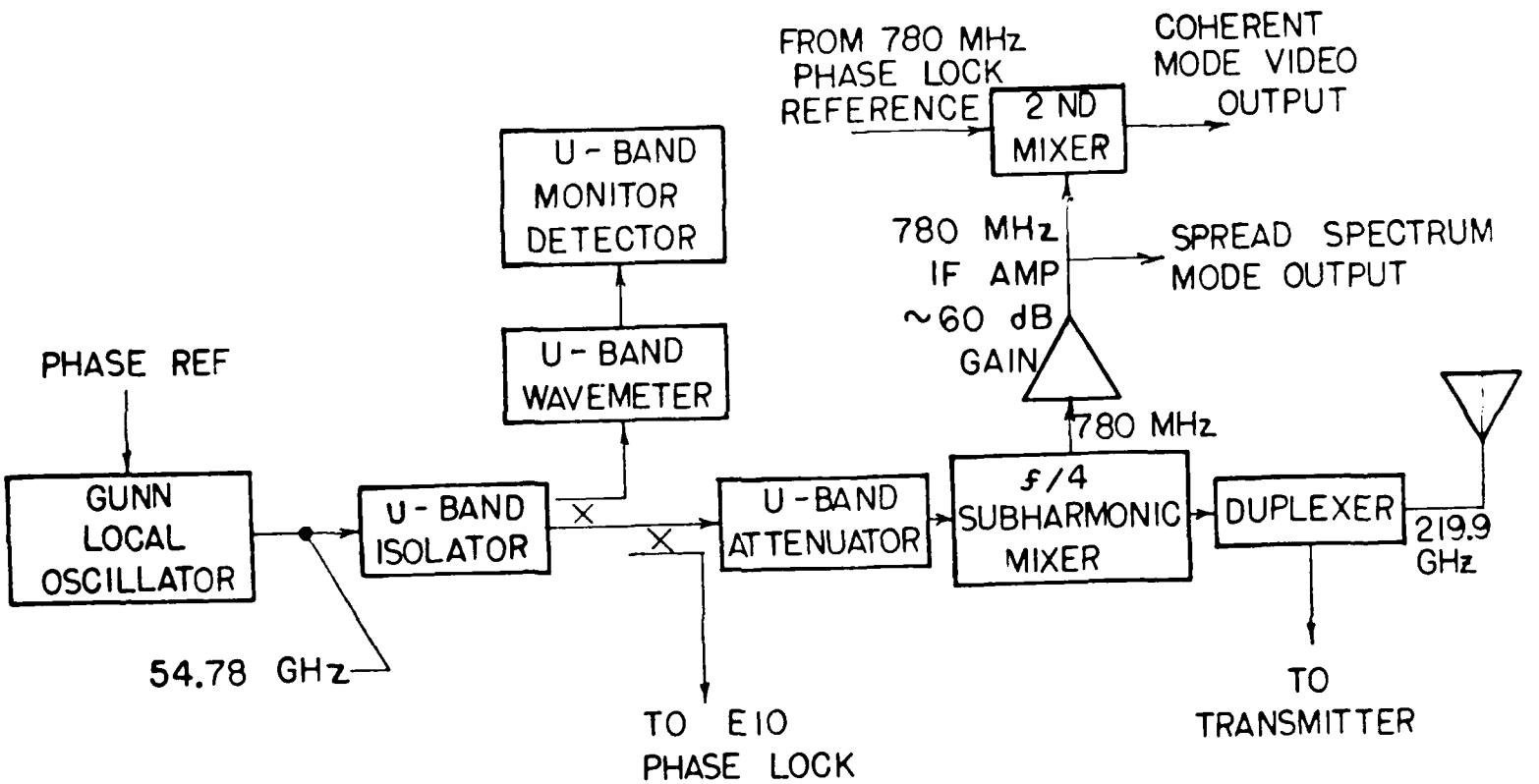

Figure 3-7. 220 GHz NMMW Radar Receiver Block Diagram.

4.0 DUPLEXER, ANTENNA, AND GIMBAL SYSTEM

4.1 Duplexer

The duplexer or transmit-receive switch provides a means of using the same antenna for transmitting and receiving in a radar system. A good duplexer should therefore have low loss in both transmit and receive paths and adequate isolation of the receiver from the transmitter output to avoid receiver damage. The duplexer approaches considered for this system were (1) the frustrated total internal reflection (FTIR) duplexer, (2) the four-port ferrite circulator, and (3) a duplexer based on transmitting circular polarization of one sense and receiving on the opposite sense. Duplexers of types (2) and (3) would probably also require an extra switch in the receiver path for adequate receiver isolation. Although the third type of duplexer was chosen for the system, the other two will be briefly discussed so that a firm basis for this choice can be established.

Figure 4-1 shows the FTIR duplexer. This device uses two transparent dielectric prisms which form a cube when placed together. If there is no gap between the prisms, radiation from the EIO passes through the cube to the antenna with little attenuation. If the prisms are separated by a small amount, radiation from the antenna will be reflected into the receiver as indicated. The separation required for good isolation is about one wavelength or 1.4 mm at 220 GHz. This duplexer approach was rejected because it is not possible to move the large prisms fast enough ($\sim$ 1 μs) to ensure that radiation from near targets will be collected by the receiver.

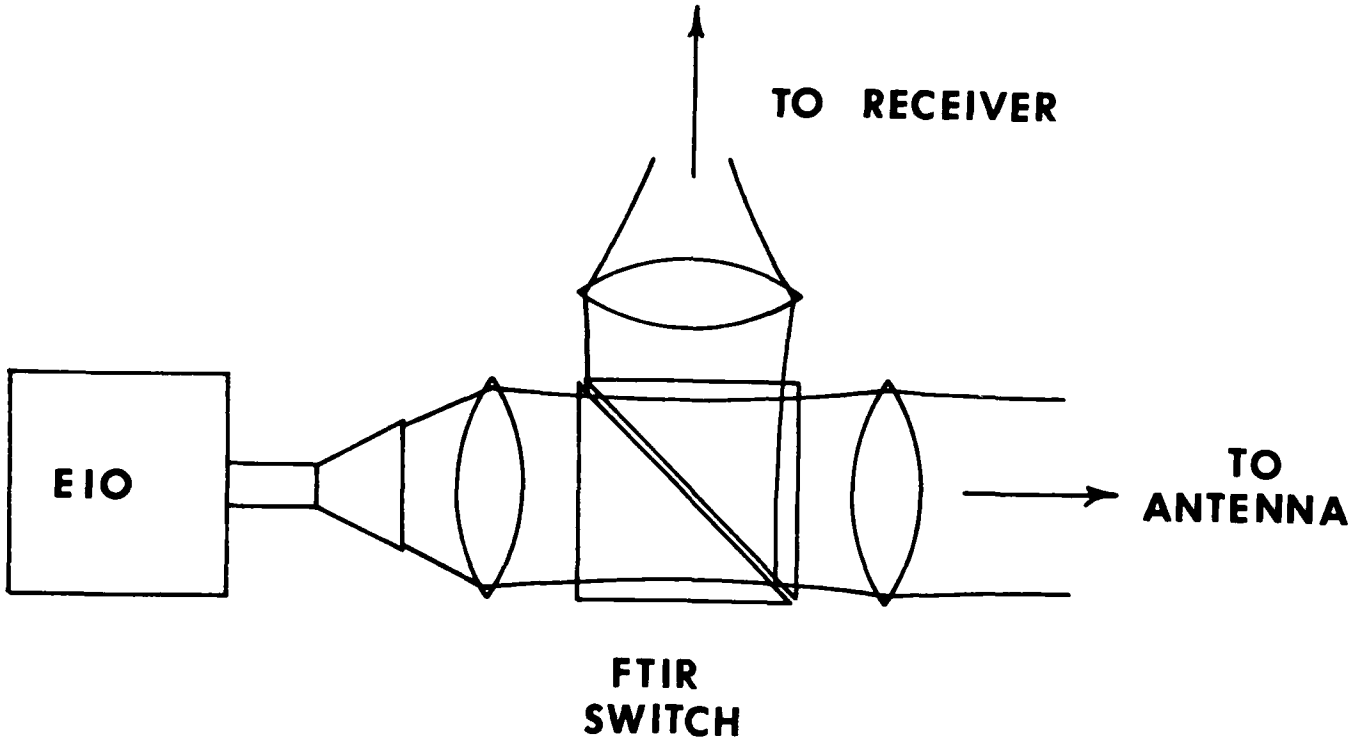

Figure 4-1. Schematic Diagram of FTIR Duplexer.

The circulator duplexer was discussed in Section 2.5 and is shown in Figure 2-9. The circulator has the property that radiation put into one of its ports is ideally emitted only from the next sequential port. In this way, a four-port circulator may be used both for injection locking and for separation of transmitter and receiver signals. The performance of these devices is measured by the isolation of radiation from unwanted ports and by the loss between sequential ports. The device considered for this system would have an isolation of 15 dB and a loss of 3 dB between ports. In addition, the waveguide switch required for receiver isolation would have a loss of 3 dB in the "on" state and 35 dB of isolation in the "off" state. Taken together, these performance figures give 3 dB loss for the transmitter path and 6 dB loss for the receiver path together with 50 dB of isolation. It was decided that these losses are intolerable when added to other system losses, and the ferrite circulator approach was rejected on that basis.

The duplexer finally chosen for use in this radar system is shown schematically in Figure 4-2 which is drawn to approximately 1/4 scale. The operation of this subsystem will be discussed in some detail in the following sections.

4.1.1 Principle of Operation

As shown in Figure 4-2, radiation emitted from the transmitter, polarized parallel to the page, is focussed by a lens onto a wire grid beam divider with wires oriented perpendicular to the page. For radiation polarized perpendicular to the wires, this grid has almost no attenuation, so that the radiation is reflected from the 45°

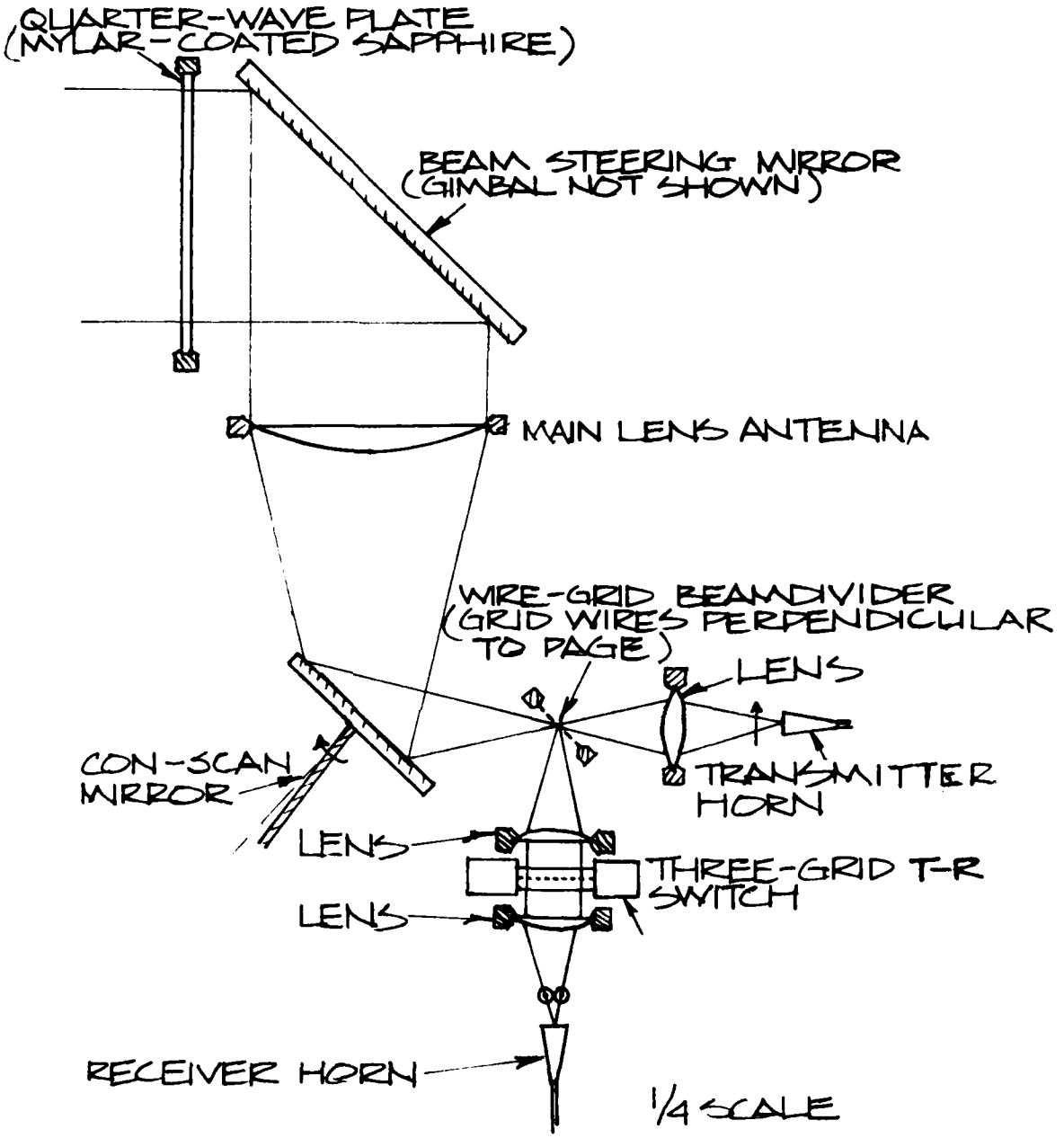

Figure 4-2. Duplexer, Antenna, and Beam Steering System to be Used in the 220 GHz Radar.

conscan mirror, collimated by the main lens antenna, reflected from the beam steering mirror, and passes through the sapphire quarter-wave plate, emerging as circularly polarized radiation. Upon reflection from the radar target, the sense of this circular polarization is reversed, and linear polarization perpendicular to the plane of the page is obtained after passing through the quarter-wave plate. This radiation follows the same path as before until it reaches the beam divider, where it is reflected downward into the receiver through the receiver isolation switch. This polarization-twisting duplexer thus provides passive isolation of receiver and transmitter, based on the change of sense of circular polarization upon reflection from a radar target.

For a well-designed duplexer, the only source of stray signals from the transmitter to the receiver is from the second surface of the quarter-wave plate, because other stray reflections will not be of the proper polarization to be reflected into the receiver by the wire-grid beam divider. To minimize reflections, the quarter-wave plate will be anti-reflection coated with mylar. In this way, it is expected that power reflected into the receiver will be about 22 dB below the transmitted power. The T-R switch will provide additional isolation. This switch, together with the different anti-reflection coatings to be used, will be discussed in the following sections.

4.1.2 Receiver Isolation Switch

The receiver isolation switch must be closed during the time that the transmitter EIO is oscillating and must open in a time of about 1-2 microsecond

so that the receiver will be sensitive to targets on the order of 300 m in range. Two different approaches are being considered for this switch. Since no firm decision on the best switching method could be reached during the program study phase, these approaches will be considered in parallel until one of them proves to be best. These approaches are: (1) a three-grid switch based on a filter design by A. Saleh [5, 6], and (2) an absorption switch which uses Stark modulation of a gas with an absorption line near the transmitter frequency. Each of these methods will be briefly discussed.

The transmission and reflection properties of the three-grid array shown in Figure 4-3 have been treated in detail by Saleh. In this figure, ϕ_1 and ϕ_2 are phase shifts between grid pairs, θ is the angle of orientation of the center grid, and input radiation is assumed to be polarized perpendicular to the wires of the two outer grids. In this configuration, the array has been shown to have peculiar transmissive properties, as shown in Figure 4-4. If $\phi_1 = \phi_2 = m\pi$ where m is an integer the transmission of this filter is zero, but if the center grid is displaced slightly in such a way that the phase shifts are unequal, the transmission rapidly approaches unity. Figure 4-4 shows that this displacement need only be about 3 microns to give essentially unity transmission. The problem of building a T-R switch using a 3-grid array then reduces to the problem of moving a single grid a distance of 3 microns in about 1 or 2 μs.

It is not difficult to show that it will not be possible to mechanically displace a free-standing wire grid in accordance with the requirements given above. Bowing of the wire grids during switching can be reduced, however, if

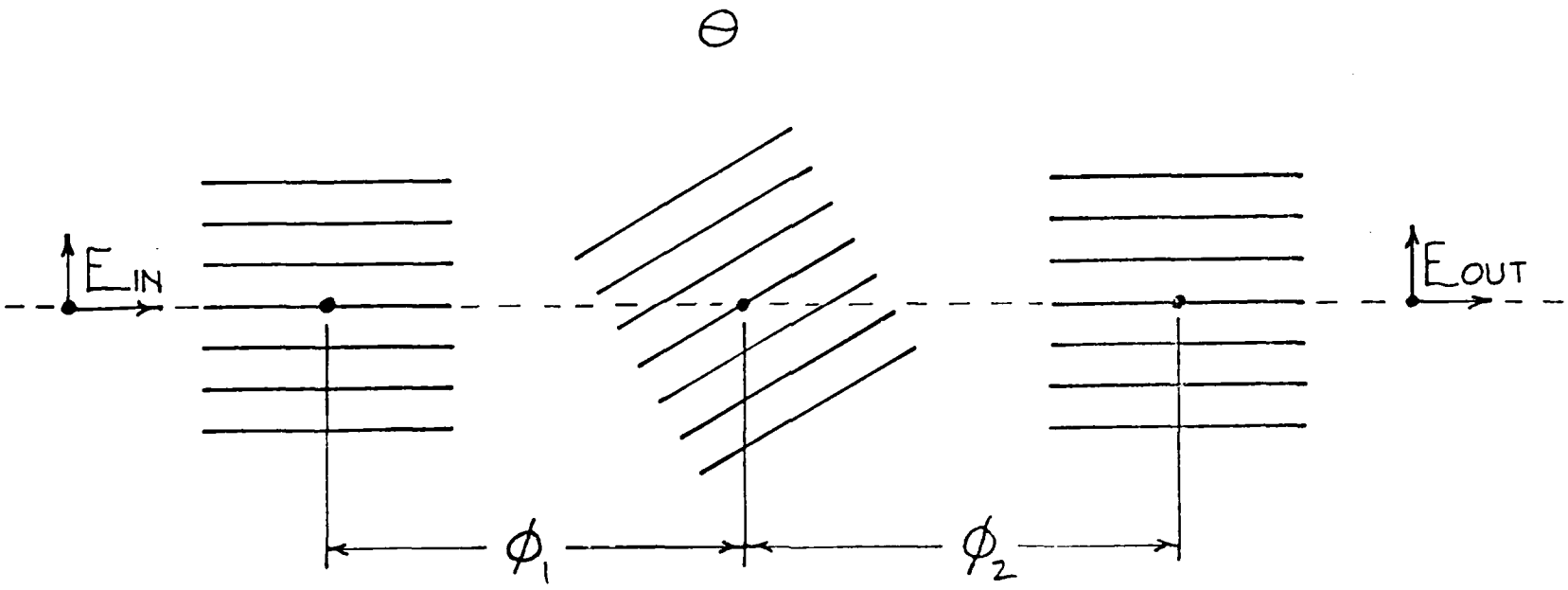

Figure 4-3. Three Grid Array Used as a Filter or Electro-Optic Switch.

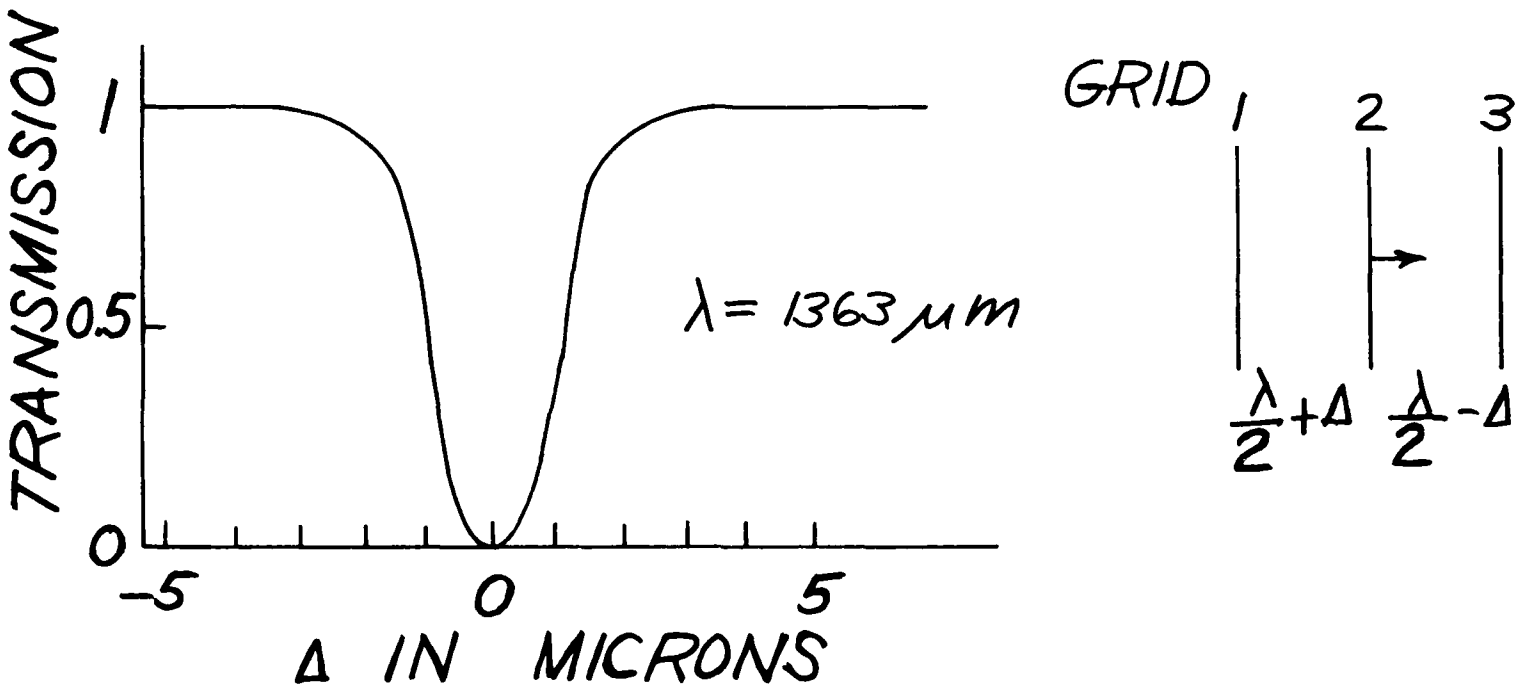

Figure 4-4. Calculated Transmission of the Three-Grid Array as a Function of Δ. The Center Grid is Oriented at 85° and $\lambda/2 + \Delta$, $\lambda/2 - \Delta$ are the Spacings between Grids 1, 2 and 2, 3 Respectively.

they are formed on a suitably stiff substrate. An apparently better approach is to place an electro-optic phase shifter in one of the gaps between grids, to change the optical path length. Either a Kerr or Pockels effect cell configuration would be suitable, depending on the availability of materials with low loss and large electro-optic coefficient. At this time the best candidate appears to be the electro-optic material lithium niobate, although some additional study must be carried out before a final choice is made.

The Stark modulation switch would use a sealed Stark cell between interferometer plates to switch the receiver radiation, as shown in Figure 4-5. The interferometer is necessary to increase the optical path by an amount sufficient to give adequate absorption. A gas with an absorption line near the transmitter frequency and with a suitable electric dipole moment is placed in the cell. The gas pressure may be varied to give an optimum absorption linewidth. With a field of a few thousand volts the absorption line is split and one of the components is tuned to coincide with the frequency of the transmitted signal. Then radiation incident from the left in the figure is heavily absorbed, but when the field is removed transmission of the signal to the receiver mixer occurs. As with the electro-optic approach outlined above, some study is required before a suitable gas can be decided upon, but it appears that methyl cyanide (CH_3CN), which has an absorption line at 220.6 GHz and gives a first-order Stark effect, is a likely candidate.

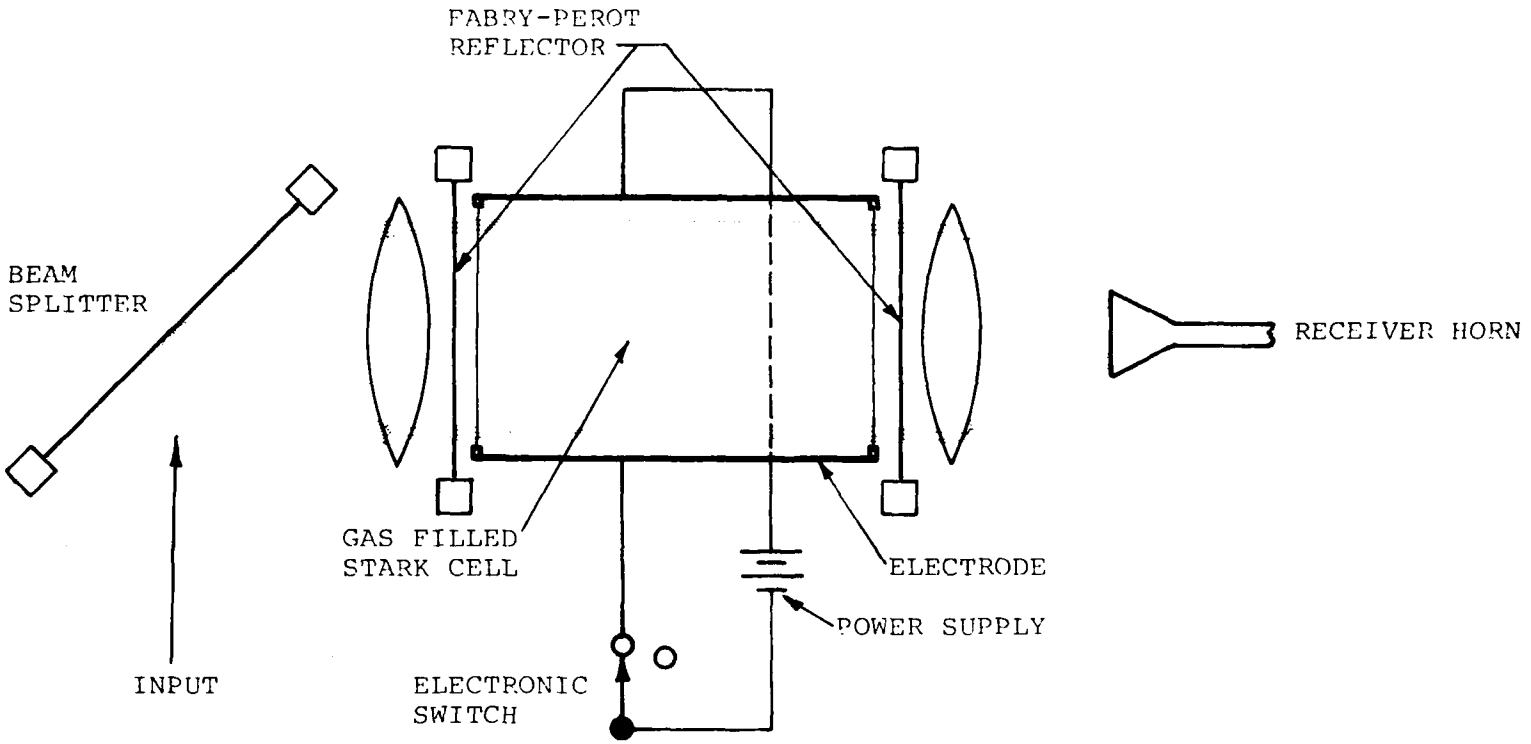

Figure 4-5. Schematic Diagram of Stark Modulation Switch.

4.1.3 Optical Matching

In any optical system containing several transmissive elements, it is necessary to anti-reflection (AR) coat each surface to minimize losses. At optical wavelengths, coatings are easily applied by vacuum deposition of thin dielectric layers, but for millimeter waves, the matching layer thicknesses are too great for this type of application. The problem of AR coating surfaces of transmissive elements used in this millimeter wave system must then be solved by choosing transparent coating materials having dielectric constants equal to the square root of that of the element to be coated, and bonding a quarter-wave thickness of this matching material to the element. Table 4-I shows several substrates and coatings that may be used in this system.

Another method of matching transmissive elements involves machining quarter-wave deep grooves in their surfaces in such a way that the average dielectric constant is equal to the square root of that of the basic material. Table 4-I shows that TPX must be matched in this way because its low dielectric constant of 1.48 would require a matching layer with a dielectric constant of 1.22, and no such material with good 220 GHz transmission is known to be available.

Note that suitable matching techniques are available for all materials of interest for this system. Losses due to reflection, absorption, and diffraction will be considered in the next section.

TABLE 4-I. USEFUL 220 GHz OPTICAL MATERIALS AND POSSIBLE ANTIREFLECTION COATINGS FOR THEM

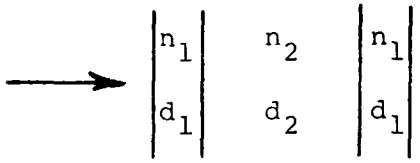

SUBSTRATE	COATING	d_1 (mm)	d_2 (mm)	n_1	n_2	R	dB
QUARTZ	TPX	0.230	7	1.48	2.12	5.4×10^{-4}	-33
SAPPHIRE	MYLAR	0.200	1	1.7	3.24	6.4×10^{-3}	-22
TPX	MACHINED GROOVES	-	-		1.48	2.0×10^{-3} EST.	-27 EST.

4.1.4 Losses

Optical path losses in this radar system may be characterized as absorption, reflection, and spill-over or diffraction losses. These losses have been calculated for both transmitter and receiver paths and are summarized in Tables 4-II and 4-III, respectively. Absorption losses were obtained from available measured data. In some cases, it was necessary to extrapolate from values measured at somewhat shorter wavelengths, but the numbers used are considered to be reasonably accurate for 220 GHz. Reflection losses were calculated from known refractive indices; again, some of these results were obtained at shorter wavelengths, but are also considered accurate at 220 GHz. It should be pointed out that Georgia Tech has the capability of measuring both absorption and refractive index of these materials and will do so, if necessary, with an optically pumped laser or other suitable source.

The total transmitter path loss is 2.2 dB, which means that only about 36 W from the 60 W EIO transmitter will be available at the antenna. The receiver path loss is estimated to be 3.7 dB. This number will add directly to the receiver mixer conversion loss and the IF amplifier noise figure to give a total system noise figure. The goal for this noise figure, as stated in the proposal, is 12 dB. Both transmitter and receiver path losses are greater than those presented during the design review because it has been decided to increase the 1/e field intensity radius of the beam incident on the antenna lens from 7.5 cm to 9.0 cm. This increases the spillover loss from 0.63 dB to 1.25 dB as shown in Table 4-IV, but gives a narrower transmitted beam.

TABLE 4-II. SUMMARY OF TRANSMITTER LOSSES

	SPILL-OVER	ABSORPTION	REFLECTION	TOTAL
FIRST LENS	1.2%	2%	0.2%	3.4%
WIRE GRID	0	0.2	0.1	0.3
CON-SCAN MIRROR	1	0.1	N/A	1.1
ANTENNA LENS	25	2	0.2	27.7
BEAM STEERING MIRROR	1	0.1	N/A	1.1
QUARTER-WAVE PLATE	1	5	0.3	6.3
			TOTAL	39.9%
			OR	2.2 dB

TABLE 4-III. SUMMARY OF RECEIVER LOSSES

	SPILL-OVER	ABSORPTION	REFLECTION	TOTAL
QUARTER-WAVE PLATE	1%	5%	0.3%	6.3%
ANTENNA LENS	25	2	0.2	27.7
CON-SCAN & BEAM STEERING MIRRORS	2	0.2	N/A	2.2
WIRE GRID	0	0.2	5*	5.2
LENS	1.2	1	0.2	2.4
T-R SWITCH	1	10 (EST.)		11
LENS	1.2	1	0.2	2.4
			TOTAL	57.2%
			OR	3.7 dB

*A 5% Loss Due To Imperfect Reflection.

Table 4-IV shows how the spillover loss is determined. This table clearly shows the trade-off between spillover loss, beamwidth, and sidelobe level. Narrow beam profiles incident on the lens antenna give low spillover and small sidelobes, but result in output beams with large divergences. Broad beam profiles result in large spillover, large sidelobes, and narrow beam divergences. The beam of radius of 9.0 cm chosen at the design review would result in a half-power beamwidth of 11 mrad, a sidelobe level of -20 dB, and a spillover loss of 1.25 dB or 25%.

4.2 Antenna and Gimbal System

4.2.1 Configuration

Figure 4-2 shows the complete antenna and gimbal system. The gimbal system is being built by Carson Astronomical Instruments of Albuquerque, N.M. and final details of its construction are not yet available. It is anticipated that a design review for this subsystem will be held early in 1980 and more detail will be available at that time.

The antenna is basically a horn-lens type which uses corrugated transmitter and receiver horns to give symmetrical E and H plane patterns and to reduce sidelobes. The lens will be machined from TPX for low loss, and will be matched by machining grooves in its surface to minimize reflection losses. Since millimeter wave lenses can be machined instead of lap ground, it is possible to fabricate them with a hyperbolic cross section, thus eliminating spherical aberrations. The lens antenna was chosen instead of reflector types because the central obscuration present in Cassegrain antennas, for example, increases the sidelobe level.

TABLE 4-IV. ANTENNA POWER DISTRIBUTION

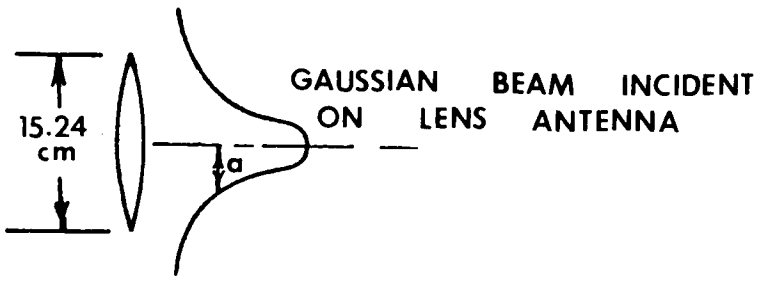

$\frac{a}{70}$ 1/e FIELD INTENSITY RADIUS CM	HPBW MRAD	SPILL-OVER LOSS dB	SIDELOBE LEVEL dB
∞	9	∞	-18
9.0	11	1.25	-20
7.5	14	0.63	-22
6.9	15	0.41	-25
5.9	17	0.18	-30
5.0	20	0.04	-40
3.6	28	4.0×10^{-3}	-60
0	∞	0	-∞

4.2.2 Search Mode

The antenna will be required to search a solid angle of 7.5° x 15° in 2 seconds. The best way to accomplish this scan based on current thinking is to scan in elevation and step in azimuth. This format takes advantage of the angle doubling effect which exists when moving the scan mirror in elevation. Taking account of this effect, the scanning mirror need move only $\pm$ 1.9 degrees to scan the 7.5 degree elevation field.

It will probably be necessary to scan both axes with a sine wave drive to minimize possible degradation caused by mechanical shock and vibration resulting from rapid directional changes at the extremes of the scan. This can be implemented by simply attaching cranks to the outputs of torque motors which drive the azimuth and elevation scan axes. However, the final approach will be determined in collaboration with Carson Astronomical Instruments, as stated earlier.

4.2.3 Track Mode

Although development of a tracking radar system with appropriate data processing is outside the scope of this effort, provision must be made in the gimbal/antenna system to accommodate this mode of operation at a later date. Since a monopulse tracker would be difficult and expensive, if not impossible, to build at 220 GHz, this radar system will use a conical scan tracker. The antenna beam is scanned in a conical format by rotating the 45° con-scan mirror shown in Figure 4-2 slightly off-axis. Most conical scanning systems use a 3 dB crossover, that is, the

power measured along a line drawn through the antenna axis is 3 dB below the main lobe peak power measured at the same distance from the antenna. The angle between main lobes would then equal the half-power beamwidth, or about 11 mrad.

In operation, the antenna would scan in search mode until a target was detected. The coordinates of this target would then be used to steer the antenna to the proper direction and the conscan track mode would be initiated. By suitable processing of the signals received in this conscan mode, it will be possible to track the target to the required accuracy, namely $\pm$ 0.5 mrad.

5.0 RADAR SIGNAL PROCESSING

An objective of this investigation is the design and fabrication of a coherent radar system operating in the near millimeter wave region at 220 GHz. This section of this technical report addresses the characteristics of the transmitter/receiver module, as driven by the specified operational goals, from the point of view of radar data processing. The bipolar video output signal of the radar receiver is then to be processed, to reduce signal-to-interference effects prior to target detection and, ultimately, tracking.

Table 1-I summarizes the system specifications which impact the transmitter/receiver configuration. The antenna aperture dimension is derived from operational considerations regarding a tank mounted application. The scan sector is rectangular, and the surveillance operation is to be completed in two seconds. Range resolution corresponding to 20 meters ($\pm$ 10 meters) is specified for target detection, when the radial component of the target velocity is between 2 and 50 kilometers per hour. Target detection at three kilometers is specified under clear air conditions, while only 1.5 kilometer target detection is required under inclement weather (fog) conditions.

5.1 Scan Considerations

For the following analyses a linear, constant rate, raster scan is assumed over the scan sector, with zero turn-around time at the sector boundaries, as shown in Figure 5-1. This scan pattern implies a beam raster scan rate of 94 degrees per second. For a pulse repetition

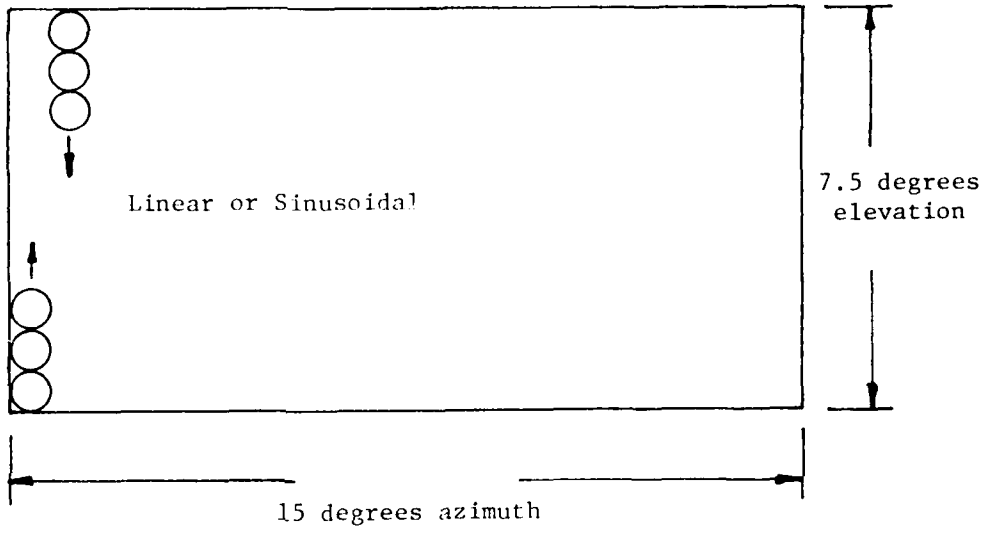

Figure 5-1. Surveillance Scan Sector and Raster Pattern.

frequency of 5,000 pulses per second, there will be some 32 hits per dwell time of 6.4 milliseconds. If the dead time on antenna turn-around at the sector boundaries is significant, the raster scan rate must be increased, and the number of hits per dwell time will correspondingly decrease. If the raster scan rate is sinusoidal rather than linear, the raster scan rate in the center of the scan sector (worst case) will be 1.58 times faster than the linear raster scan rate (no dead time), resulting in only approximately 20 hits per dwell time on a target. Two second sector coverage is assumed for both linear and sinusoidal raster scan rates. However, increasing the number of hits per dwell time (with a sinusoidal raster scan rate) back to 32 can be effected by either increasing the PRF, increasing the sector scan time, or widening the beamwidth. But each of these options imposes its own particular requirements on system operation which may not be compatible with system performance goals. For example, a higher PRF may require a more powerful modulator power supply, assuming that the power oscillator (an FIO) is not already duty factor limited. Increasing the sector scan time decreases the overall coverage rate of the radar, which is usually undesirable. Likewise, widening the beamwidth degrades the spatial resolution of the radar.

The impact of the raster scan rate on signal processing will be through the dwell time on a target and, therefore, the number of hits during this dwell time. Assuming FFT signal processing, the processor Doppler resolution will equal the inverse of the dwell time, where the dwell time corresponds to the number of data points used in the FFT processing. For a PRF of 5,000 pulses per second and a linear raster scan rate, the dwell time of 6.4 milliseconds corresponds to 32 hits on a target. Thus a 32-point FFT

signal processor may be used for signal-to-interference (clutter plus noise) reduction. The resulting processor Doppler resolution is thus 156 Hz, which corresponds to a target radial velocity resolution of approximately 0.4 kilometers per hour. Note that the range of Doppler frequencies which corresponds to the range of target radial velocities (2 to 50 kilometers per hour) is from 815 to 20,370 Hz for the 220 GHz radar frequency.

Another impact on system performance will be the generation of blind speeds at target radial velocities of 12.3, 24.5, 36.8, and 49.1 kilometers per hour. Furthermore, target Doppler frequencies will be ambiguous due to frequency foldover. Both effects result from using a sampling rate of 5,000 Hz (the PRF) for signals with frequencies up to 20,370 Hz.

5.2 Fully Coherent System

The essential modular relationships making up the fully coherent transmitter/receiver system of the radar are depicted in Figure 5-2. This figure is similar to Figure 1-1, but is simplified to show the features relevant to signal processing. A very stable 97.5 MHz source serves as the master reference oscillator for the entire transmitter/receiver. The coherent oscillator (COHO) signal is generated from the reference signal using a phase locking circuit which is tuned to 780 MHz (8 x 97.5 MHz). The PRF signal is simply counted down from the reference signal and is, therefore, synchronized to the reference signal.

The stable local oscillator (STALO) signal is generated from the reference signal using a GUNN oscillator tuned to 54.8 GHz which is phase locked to the reference signal by using a medium power source with some convenient intermediate frequency. The extended interaction oscillator (EIO) output signal is synchronized to the reference

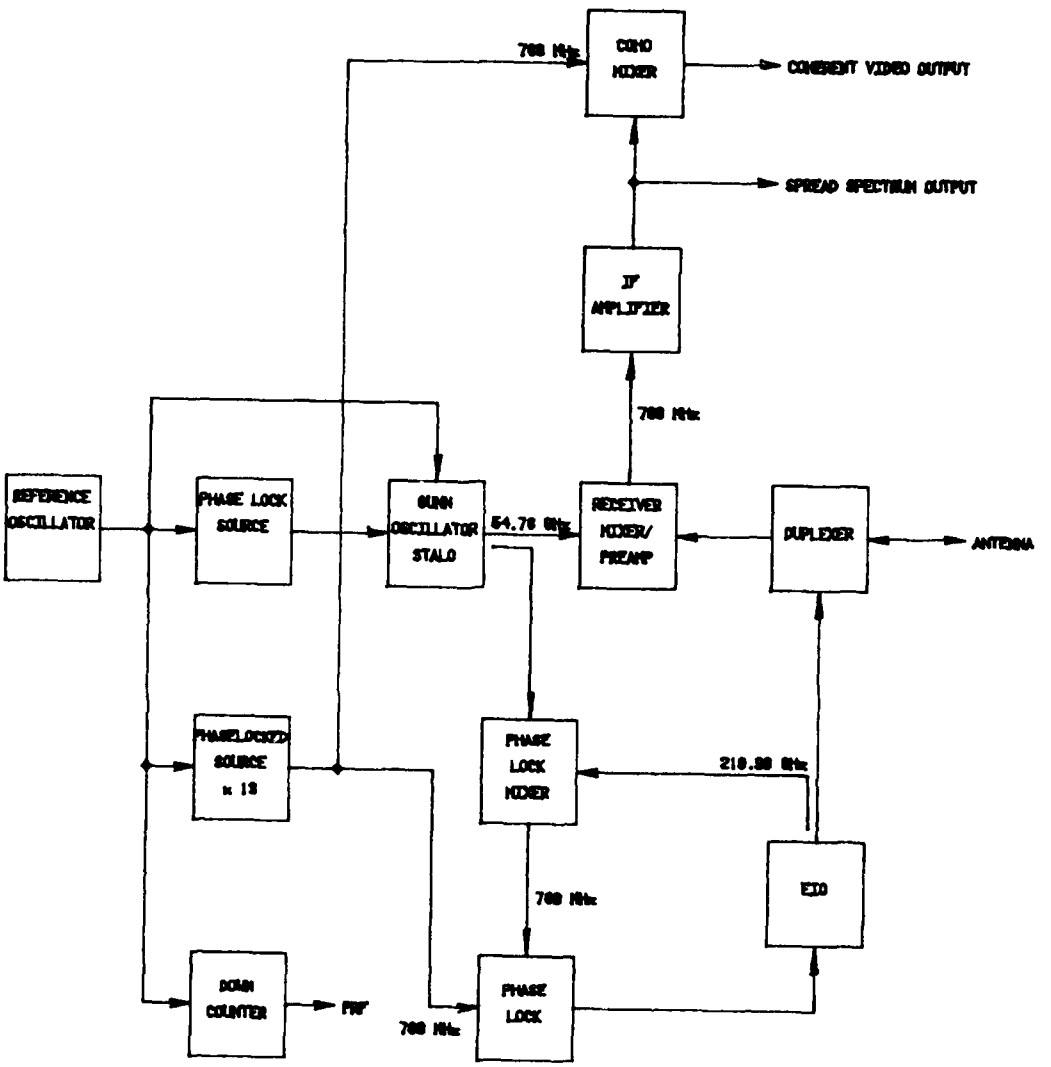

Figure 5-2. 220 GHz Coherent Radar Block Diagram.

oscillator by downconverting a sample of the EIO output signal, which is mixed with the STALO signal in a 4X mixer, and phase comparing the mixer output with the reference signal to generate an EIO correction signal.

The received signal is downconverted to the intermediate frequency (IF) using another 4X mixer and the STALO output. The 780 MHz IF signal is amplified (linear transfer function) prior to being coherently detected, with respect to the COHO signal, using a conventional mixer. The linear amplifier should supply 30 to 40 dB signal gain and have a bandwidth matched to the transmitted pulse length. Thus, for a 50 nanosecond pulse length, the receiver (IF amplifier and associated filter) bandwidth would be approximately 20 MHz, while a longer 200 nanosecond pulse length would require about a 5 MHz bandwidth receiver to maximize the amplitude output signal-to-noise ratio.

The output of the coherent detection process is a bipolar video signal whose amplitude represents target reflectivity and whose (Doppler) frequency represents target motion radial to the radar. This video signal will then be the input signal for a signal processor, whose function will be to enhance the target-to-interference ratio for target detection and target tracking.

5.3 Non-Coherent System

An alternative modular relationship is depicted in Figure 5-3, showing a non-coherent transmitter/receiver system. The essential difference between the non-coherent and fully coherent configurations is that in the non-coherent case the "second detector" is a diode type detector whose output signal is essentially the envelope of the IF

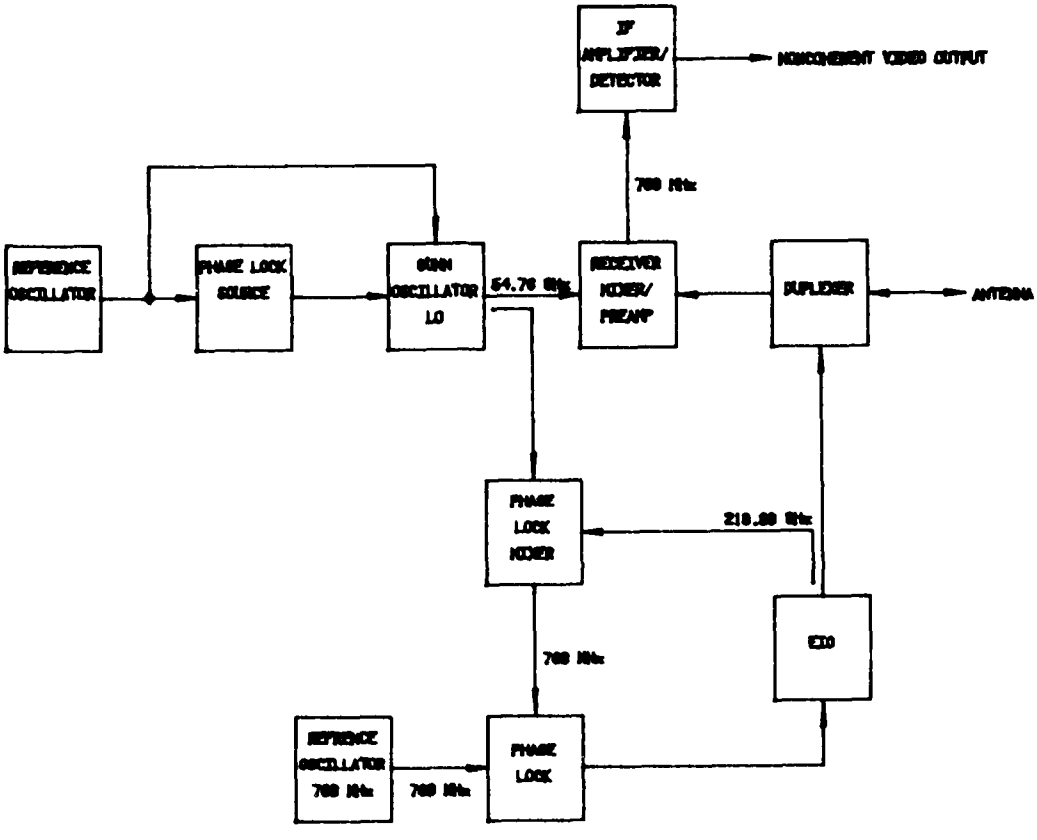

Figure 5-3. 220 GHz Non-Coherent Radar Block Diagram.

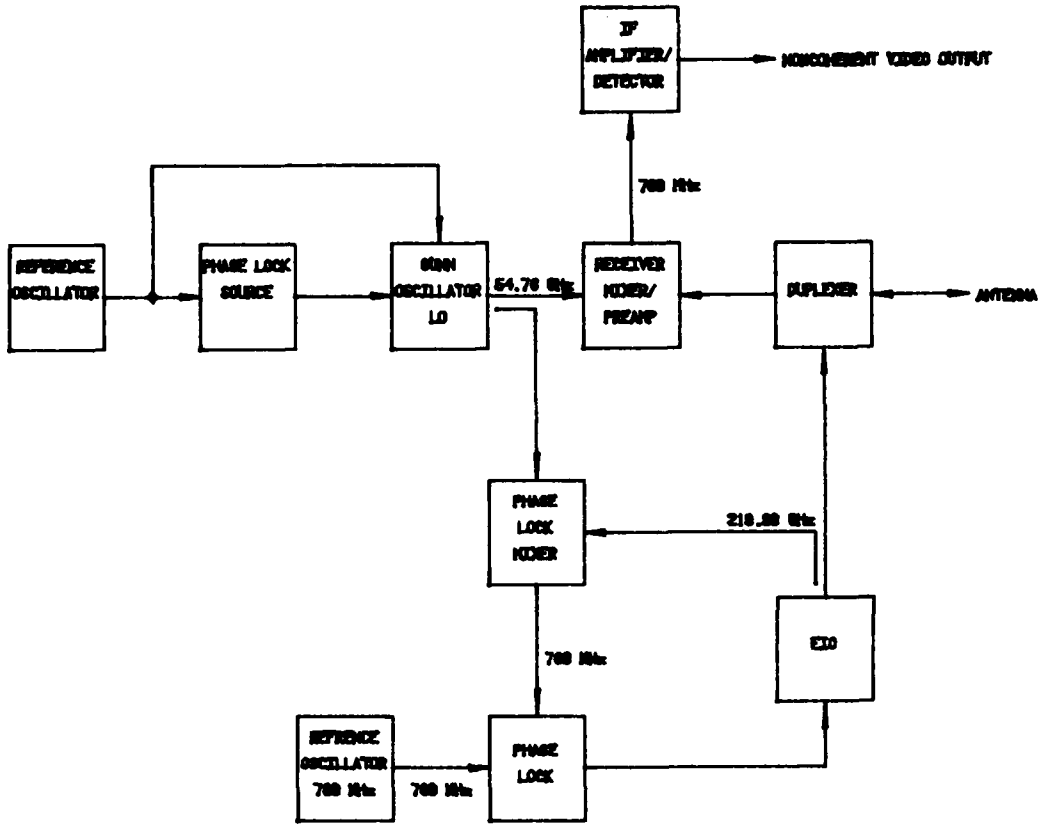

Figure 5-3. 220 GHz Non-Coherent Radar Block Diagram.

input signal. No phase information (Doppler frequency) is present in the output of the non-coherent mode of operation. The non-coherent radar output signal is unipolar video, for eventual data processing. In contrast, the coherent configuration "second detector" is a mixer, and the output signal is bipolar and retains amplitude and phase information.

The non-coherent configuration is a fall-back design in case the EIO frequency stability (intrapulse FM) does not permit adequate coherent radar operation. EIO FM will cause the target return signal to have a correspondingly wider bandwidth since the STALO frequency is fixed during the interpulse period. The increased target return bandwidth due to EIO FM requires an increased bandwidth IF amplifier, resulting in a degraded target-to-noise signal ratio. Furthermore, FFT processing of non-coherent video signals will result in less signal-to-interference enhancement than for coherent video since non-coherent target returns will be spread out over several frequency bins. More specific processing improvement estimates for both configuration cases are additional tasks to be addressed.

5.4 Signal Processing Analysis of 220 GHz Coherent Radar

Pulse Doppler (PD) processing is the preferred signal processing approach for the 220 GHz near millimeter wave coherent radar. Although more expensive and complex than delay line canceller type moving-target-indicator (MTI) processing techniques, PD processing has the capability to extract more information from the radar returns. PD processing provides target range-rate discrimination and an

increased signal-to-noise ratio, S/N, via coherent integration, resulting in increased target detection capability. The implementation of PD processing can involve the use of the Fast Fourier Transform (FFT) algorithm.

5.4.1 Basic Considerations

The main functions of the PD processor are, (1) to separate a moving target from a fixed clutter background, thus enhancing target detection, and (2) to determine the range rate (radial speed) of that target. A quantitative measure of a PD processor's ability to accomplish these tasks is the PD improvement factor, I; defined as the signal-to-clutter ratio, S/C, at the output of the processor divided by the signal-to-clutter ratio at the input. The PD improvement factor differs from the MTI improvement factor in that in evaluating the MTI improvement factor for an MTI processor, the output signal is averaged uniformly over all target radial velocities, i.e., Doppler frequencies of the target. Thus, the MTI improvement factor becomes a measure, in an average sense, of the performance of the MTI radar, and does not indicate improvement performance for a given target moving with a given radial speed, the Doppler return from which may occur, for example, at a minimum response frequency of the MTI processor. However, since a pulse Doppler processor provides target radial speed information, it is of interest to know the improvement factor as a function of this speed. Therefore, no Doppler frequency averaging is performed in the evaluation of the PD improvement factor.

Perfect PD processing performance requires a total elimination of the clutter signal. Any clutter residue, C_o, present at the output of the processor results in a

degradation of target detection performance. Clutter residue originates from two general sources: (1) clutter spectral broadening and (2) imperfections (instabilities) in the radar system itself. Clutter spectral broadening in a stationary radar is caused by internal clutter motion and antenna scanning motion. Radar system imperfections include variations in transmitted power and frequency, pulse width, and PRF. If I_k is the limitation in improvement factor attributable to clutter source k, then the total limitation in improvement factor, I, is given by

$$I^{-1} = \sum_k I_k^{-1}, \qquad (5\text{-}1)$$

where the sum is over all sources of clutter residue.

Limitations to improvement factor attributable to system instabilities are not considered here, since the magnitudes of the instabilities are not known at this time. However, once determined, their effect on I can easily be determined by the use of Equation 5-1.

Pulse Doppler processing can be accomplished by using FFT digital processing. A N-point FTT processor will take N samples of a signal, sampled at rate R (in this instance, R will equal the radar's PRF) for a time T = N/R, perform a discrete Fourier Transform on these samples, and arrange the results at N discrete frequencies of magnitude k/T (where k is an integer) extending in frequency from - R/2 to + R/2. Thus, the frequency resolution of the FFT processor is 1/T, i.e., a signal whose frequency f is in the frequency range of bin n, i.e.,

$$\frac{n - \frac{1}{2}}{T} < f < \frac{n + \frac{1}{2}}{T}$$

will appear in the output of the FFT processor at frequency n/T. This signal will also appear in other bins due to the finite sampling time, T, which causes the filter response of any given bin to have frequency sidelobes. However, this effect can be minimized with appropriate window weighting to reduce the sidelobe levels. The maximum unambiguous frequency determinable by the FFT processor is R/2, and higher signal frequencies present will be "folded over" into the FFT processor's frequency interval [-R/2, R/2], i.e., an arbitrary frequency f - kR + f', where k is an integer and $-R/2<f'<R/2$, will appear in the frequency bin containing f'.

The 220 GHz near millimeter radar system has the following system parameters:

Antenna Beamwidth:	0.6° pencil beam
Scan Sector:	7.5° elevation x 15° azimuth
Sector Scan Time:	2 seconds
Target Radial Speeds:	2 to 50 km/hr

Assuming a uniform antenna scan rate, these parameters result in a T = 6.4 millisecond target dwell time. Therefore, the Doppler frequency resolution (bin size) of the FFT processor would be 156.25 Hz, independent of PRF selection.

In order to unambiguously determine the radial speeds of targets up to 50 km/hr, the PRF must be at least 40.8 kHz. At this PRF no fold-over or blind speeds occur for the range of target speeds specified. This PRF also yields the best overall improvement factor, as shown by the following argument. The improvement factor increases with increasing target Doppler frequency, since the clutter is centered in

frequency around zero Doppler. For a PRF less than 40.8 kHz, the target returns with high Doppler frequencies fold-over and appear in lower frequency Doppler bins; thus, the improvement factor is reduced for these targets. No improvement factor gain is obtained by increasing the PRF above 40.8 kHz as long as 50 km/hr is the top target radial speed encountered. Increasing the PRF, however, will improve the signal-to-noise ratio.

Transmitter and/or transmitter modulator restrictions may require limiting the maximum PRF to 5 kHz. A PRF this low will result in severe spectrum fold-over. The highest unambiguous target speed would be 6.14 km/hr and blind speeds would occur at 12.3, 24.5, 36.8, and 49.1 km/hr. The number of pulses returned from a target in one sector scan is N = PRF x T = 32. Therefore a 32-point FFT processor will be adequate for the radar system with a 5 kHz PRF.

A PRF as high as 20 kHz is obtainable from the transmitter/modulator assembly. This PRF would increase the highest unambiguous target speed to 24.5 km/hr and would eliminate all blind speeds except for one at 49.1 km/hr. A 128-point FFT processor would be adequate for the radar system with a 20 kHz PRF.

In order to obtain an analytical expression for the improvement factor limitation due to clutter spectral broadening, a land clutter spectral model at 220 GHz must be obtained. This is addressed in the next section. Clutter spectral broadening due to antenna scan can be accounted for with the appropriate signal weighting and will not be considered further.

5.4.2 Land Clutter Spectral Model

No measured data exist for land clutter backscatter at 220 GHz. Experimental clutter data have been collected on trees at 95 GHz [7]. The clutter power spectrum, P(f), of trees at 95 GHz was found to be analytically modeled well by the sum of two Lorentzians (see Figure 5-4),

$$P(f) = P_L(f) + P_H(f) \tag{5-2}$$

where $P_L(f)$ models the low frequency contribution to the spectrum, and is given by

$$P_L(f) = \frac{50\,A}{1 + \left(\frac{37.5\,f}{f_c}\right)^2} \tag{5-3}$$

and $P_H(f)$ models the high frequency contribution to the spectrum, and is given by

$$P_H(f) = \frac{A}{1 + \left(\frac{f}{f_c}\right)^2} \tag{5-4}$$

This model is assumed to be valid at 220 GHz and f_c is assumed to scale linearly with radar frequency. The half-power frequency point, f_c, is 30 to 35 Hz for deciduous trees in 6 to 15 mph winds at 95 GHz. Therefore, f_c can be assumed to be approximately 75 Hz at 220 GHz.

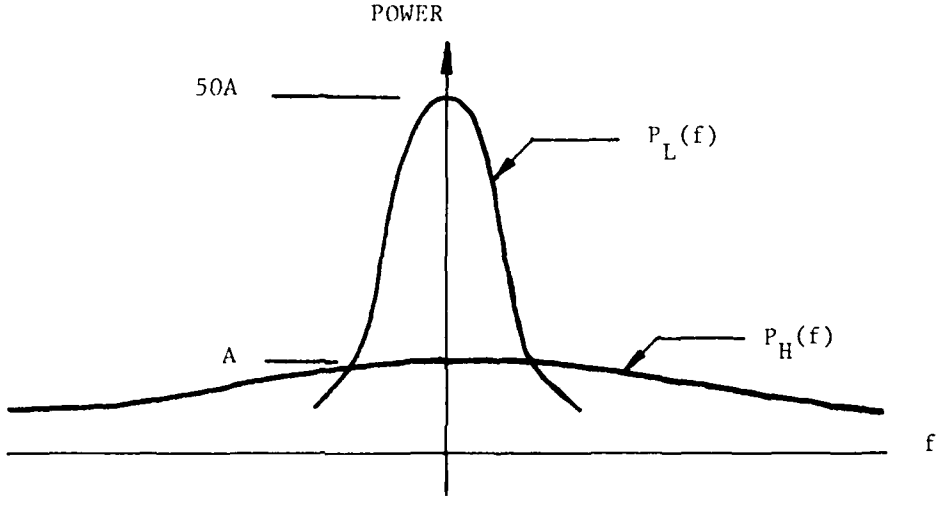

Figure 5-4. Tree Clutter Spectral Model.

5.4.3 Improvement Factor

Before an analytical expression can properly be determined for the PD improvement factor, the appropriate weighting must be applied to the received range-gated signal in order to reduce frequency sidelobe levels of the FFT filter response of any given bin. Chebyshev weighting is chosen due to its desirable attributes of uniform sidelobe level and mathematical tractability. Shown in Figure 5-5 is the filter response of frequency bin m when Chebyshev weighting (-60 dB sidelobe level) is applied. The equivalent noise beamwidth of the mainlobe is 1.51 bins. The mathematical model of this filter response that is used in the analysis is shown in Figure 5-6. A zero response notch, one-half bin wide, is included around zero Doppler to give accurate improvement factor results for those cases when the clutter spectrum is narrow enough to be contained in the sidelobe null.

Using the land clutter spectral model given by Equations (5-2), (5-3), and (5-4), and the Chebyshev weighting model shown in Figure (5-6), the PD improvement factor versus frequency bin and target radial speed is shown in Figure (5-7) for f_c = 75 Hz, PRF = 5 kHz and a 32-point FFT processor. The PD improvement factor versus frequency bin and target radial speed is also shown in Figure (5-8) for f_c = 75 Hz, PRF = 20 kHz and a 128-point FFT processor. In order to determine the improvement factor needed for the particular radar application addressed here, the radar cross section per unit area, σ^o, of the clutter must be determined.

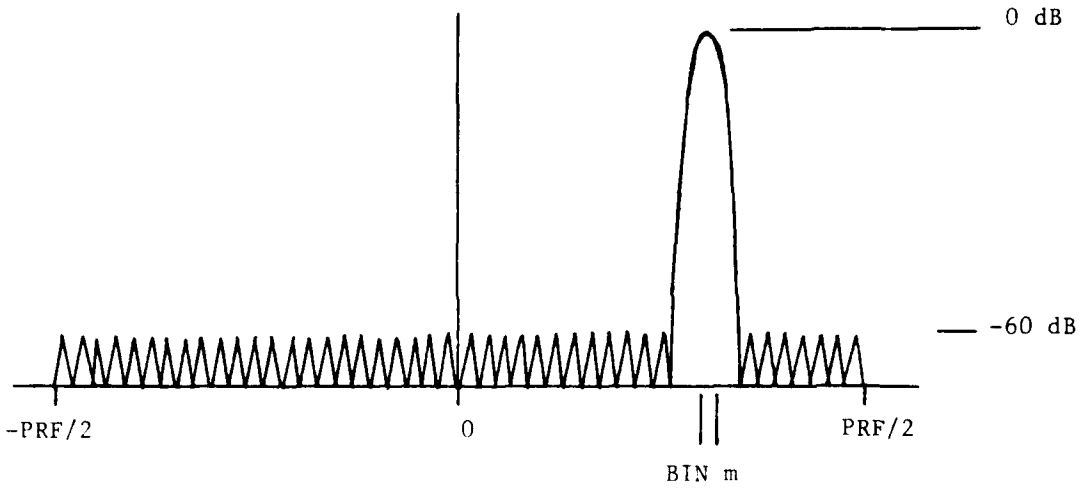

Figure 5-5. Filter Response of Frequency Bin m with Chebyshev Weighting Applied.

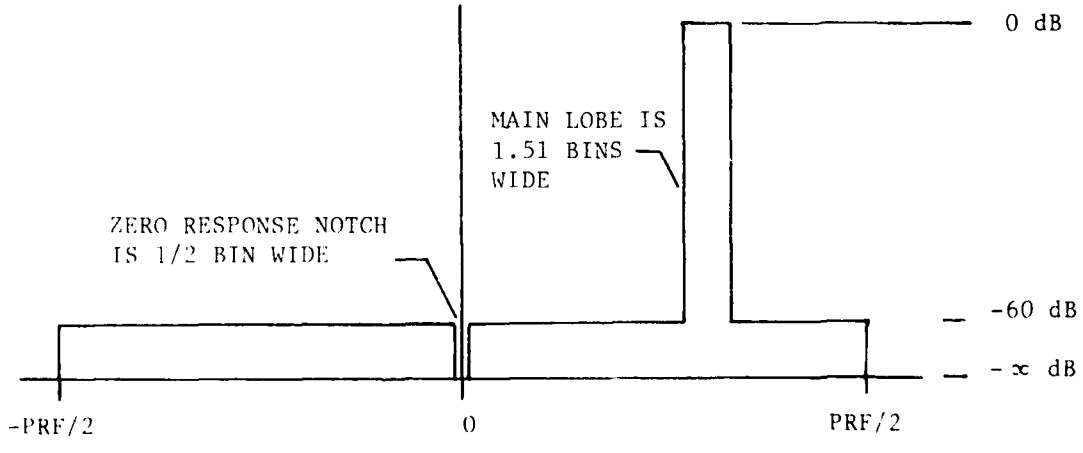

Figure 5-6. Mathematical Model of Filter Response of Frequency Bin m.

AD-A083 493 GEORGIA INST OF TECH ATLANTA ENGINEERING EXPERIMENT --ETC F/G 17/9
NEAR MILLIMETER WAVE RADAR TECHNOLOGY.(U)
JAN 80 R W MCMILLAN, R E FORSYTHE DAAK70-79-C-0108
UNCLASSIFIED NL

2 OF 2
AD A083493

END
DATE FILMED
5-80
DTIC

5.4.4 Land Clutter Model for σ^o

No measured data exist for land clutter backscatter at 220 GHz, as previously mentioned. Experimental clutter data, collected on trees at 35 and 95 GHz, resulted in the following model for σ^o for deciduous trees [8]

$$\sigma^o = -11 + 10 \log \frac{\theta}{25} - 8 \log \frac{\lambda}{.32} \quad \text{dB}, \tag{5-5}$$

where λ, the transmitted radar wavelength, is in centimeters and θ, the antenna depression angle, can vary from 1° to 45°.

This model is assumed to be valid at 220 GHz, thus σ^o = - 22 to -5 dB for $1° < \theta < 45°$. A mean value of σ^o = -14 dB is chosen for tree clutter at 220 GHz.

5.4.5 Required Improvement Factor

The signal-to-interference (noise plus clutter) ratio can be written as

$$\frac{S}{N+C} = \frac{1}{(S/N)^{-1} + (S/C)^{-1}} \tag{5-6}$$

The signal-to-interference ratio out of the signal processor, $(S/N + C)o$, must be equal to

$$\left(\frac{S}{N+C}\right)_o = \begin{cases} 19.4\,\text{dB} & P_d = 0.9 \\ 10.8\,\text{dB} & P_d = 0.5 \end{cases} \tag{5-7}$$

for the probabilities of detection, P_d, shown and for a probability of false alarm of 10^{-4} [9].

As shown in a previous section, the input signal-to-noise ratio, $(S/N)_i$, for the 220 GHz radar is approximately 0 dB for a 200 nsec. pulse, three kilometer range in warm dry air. Assuming the noise to be "white" into the processor, the processing gain, I_N, of signal-to-noise is equal to the number of frequency bins, i.e., the number of points in the FFT. Therefore, the signal-to-noise ratio out of the processor, $(S/N)_o$, is

$$\left(\frac{S}{N}\right)_o = I_N \left(\frac{S}{N}\right)_i = \begin{cases} 15.1 \text{ dB} & \text{for } 32 \text{ bins (PRF = 5 kHz)} \\ 21.1 \text{ dB} & \text{for } 128 \text{ bins (PRF = 20 kHz)} \end{cases} \quad (5\text{-}8)$$

As can be seen from Equations (5-6), (5-7), and (5-8), noise limitations prevent the detection of any moving target with $P_d = 0.9$ for the PRF = 5 kHz case.

Assuming a target radar cross section of 17 dBsm, a target range of three kilometers, a pulse width of 200 nsec., and a clutter σ^o of - 14 dB, the processor input signal-to-clutter ratio is + 1.2 dB. Therefore, from Equations (5-6), (5-7), and (5-8), and the definition of improvement factor, i.e.,

$$I = \frac{(S/C)_o}{(S/C)_i},$$

the necessary improvement factors are approximately equal to

	$P_d = 0.5$	$P_d = 0.9$	
I =	12 dB	-	PRF = 5 KHz
	10 dB	23 dB	PRF = 20 KHz

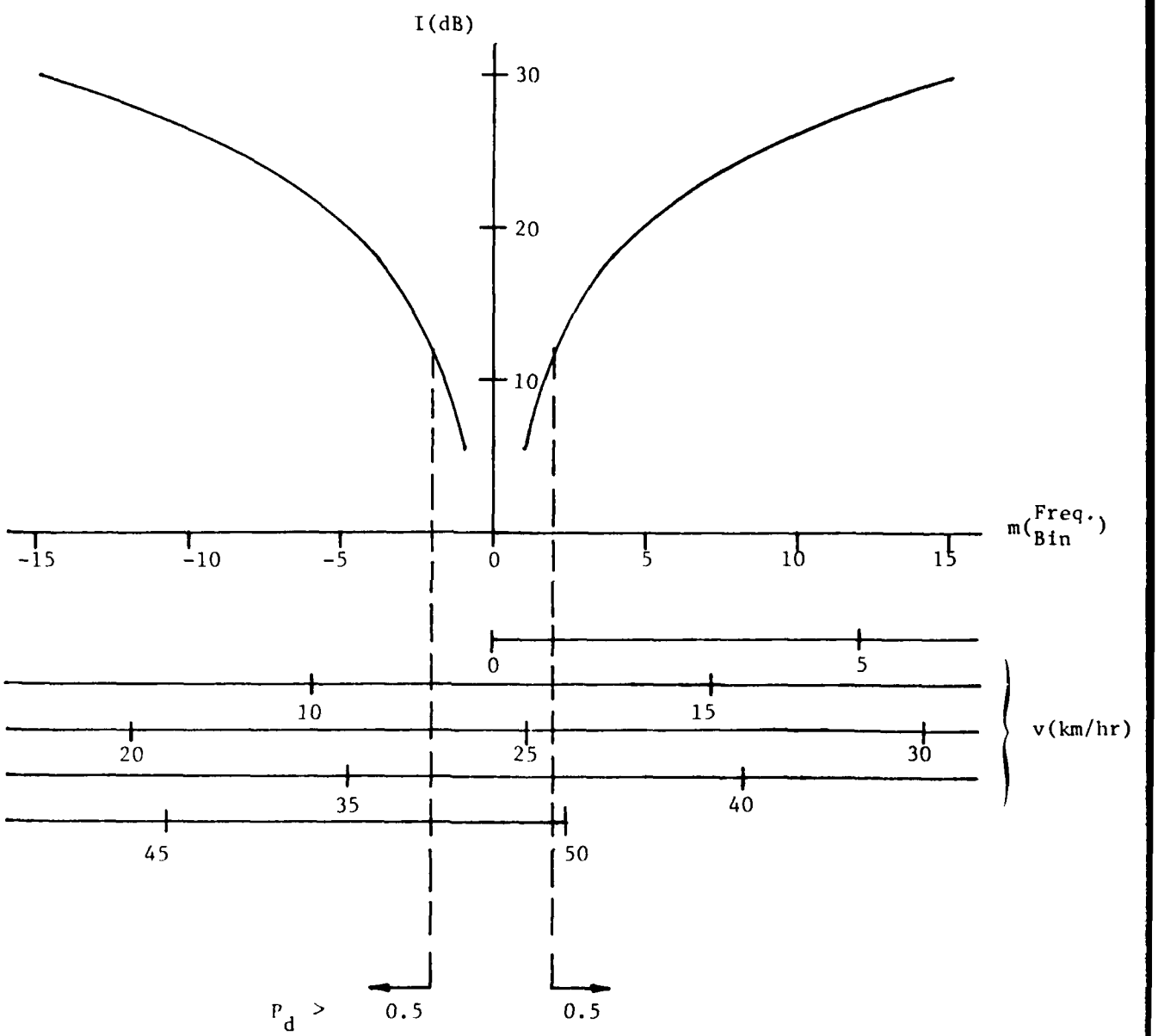

Figure 5-7. PD Improvement Factor vs. Target Speed for PRF = 5 kHz.

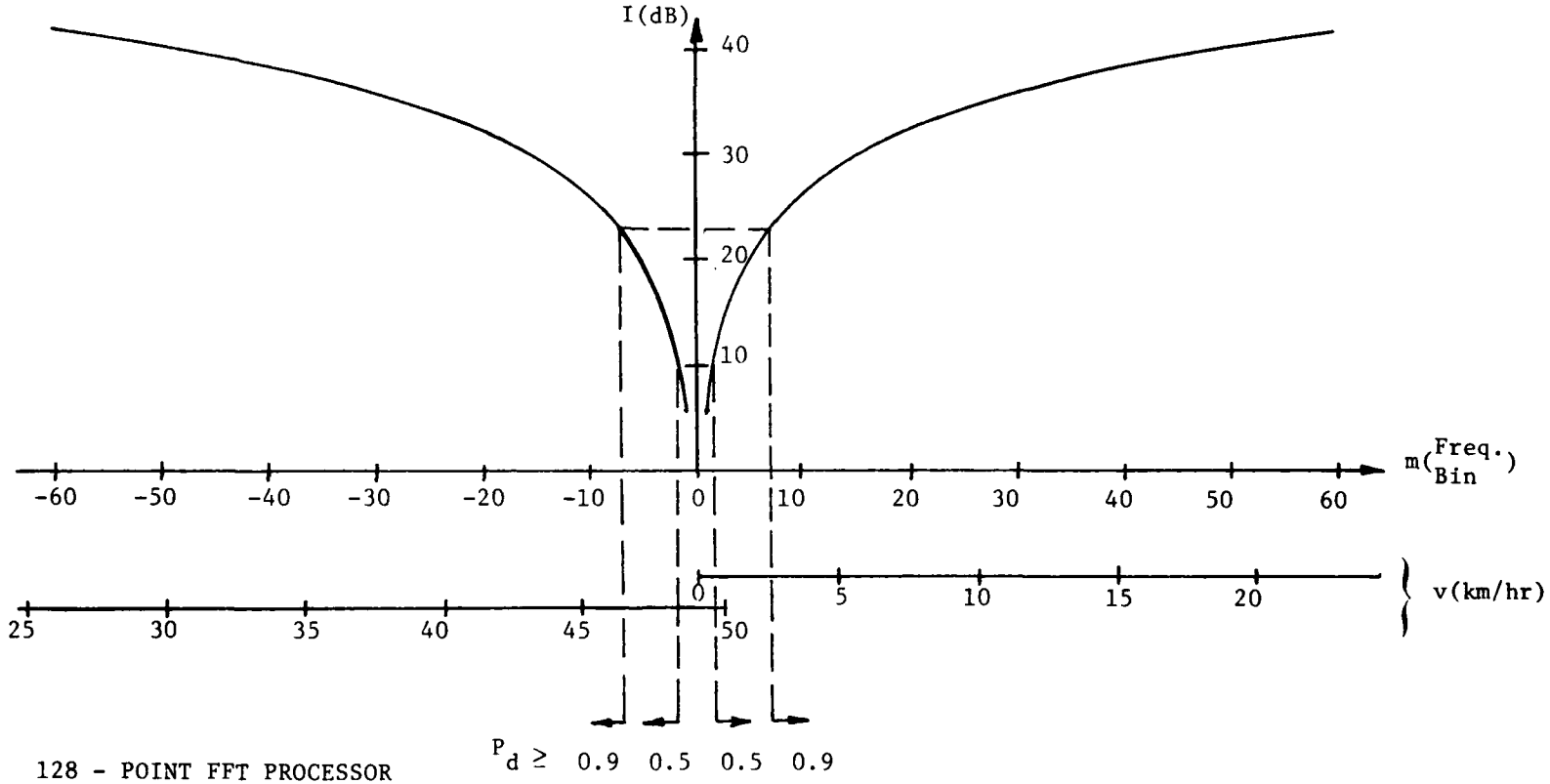

128 - POINT FFT PROCESSOR
PRF = 20000 HZ
f_c = 75 HZ (LORENTZIAN CLUTTER MODEL)
CHEBYSHEV WEIGHTING
(SLL = -60 dB, ENBW = 1.51 BINS)

Figure 5-8. PD Improvement Factor vs. Target Speed for PRF = 20 kHz.

These values for the required improvement factor are shown in Figures (5-7) and (5-8). For the 5 kHz PRF processor (Figure 5-7), approximately 10.0 percent of the specified target radial speeds lie in the below 0.5 probability of detection range. However, for the 20 kHz PRF processor (Figure 5-5), only target radial speeds from 0 to 2.5 km/hr and 46.5 to 50 km/hr lie in the below 0.9 probability of detection range, and target radial speeds from 0 to 0.6 km/hr and 48.5 to 49.7 km/hr lie in the below 0.5 probability of detection range. These speed ranges represent, respectively, only 8.3% and 2.5% of the target radial speeds specified.

A major operational limitation of operating at a PRF of 5 kHz is the inability to detect any moving target with a P_d of 0.9. As was shown, this inability is due to receiver noise limitations. If PRF's in the neighborhood of 5 kHz are the maximum that can be achieved with the transmitter/modulator assembly, then a lower P_d must be accepted. However, the four blind speeds that occur with this PRF selection may be eliminated by the PRF staggering. For example, a two-PRF stagger of 4.8 and 6 kHz gives a minimum blind speed of 58.9 km/hr. The curve of improvement factor versus target speed for such a PRF stagger is an area for further analysis.

Other areas of investigation should include the effects on the PD improvement factor due to (1) actual beam raster scanning, i.e., finite turn around times and non-constant beam scanning rates, and (2) radar system imperfections. Finally, an analysis of the processing improvement that can be expected for a non-coherent clutter-reference MTI radar system should be conducted.

6.0 SUMMARY OF PROGRAM STATUS

6.1 Procurement

All critical parts with long delivery times have been ordered. These parts are all expected to be received by 15 April 1980, with the exception of the gimbal system, which will be shipped about 1 December 1980. If our vendors meet these dates, adequate time will be available to do a proper job during the critical component development phase of the program. However, it has been Georgia Tech's experience that millimeter wave vendors tend to be late because of large backlogs. For this reason, a letter is being sent to each vendor who has delivered late in the past asking them to reaffirm their projected shipping dates and emphasizing the urgent need for on-time deliveries during this program. Table 6-I summarizes the long-lead items ordered to date and gives price and delivery information.

Components which have not yet been ordered include parts for the phase lock loop, receiver IF amplifier, and television subsystem. These items are not considered to have long delivery times, but will be ordered early in January, since additional funds have been received.

6.2 Financial

Table 6-II is the financial statement from the monthly progress report for November 1979. This statement shows an underrun of about $10K in personal services, overhead and retirement, and an overrun of $23K in materials and supplies. This overrun has since been cancelled by the addition of $300K which will be used during FY-80 for the critical component development phase of the program.

TABLE 6-I. LONG-LEAD ITEM PROCUREMENT STATUS

ITEM	VENDOR	PROMISED DELIVERY DATE	PRICE
Gimbal System	Carson Astronomical Instruments Albuquerque, N.M.	12/01/80	$83,945
Extended Interaction Oscillator	Varian of Canada Georgetown, Ontario	04/01/80	25,850
G-Band Frequency Meter	TRG Division of Alpha Woburn, MA	02/20/80	1,050
G-Band Waveguide Components	"	02/20/80	3,030
G-Band Detector	Baytron Medford, MA	04/01/80	1,500
G-Band Coupler	"	04/01/80	2,300
55 GHz Phase-Locked Gunn Oscillator	Hughes Torrance, CA	04/15/80	8,820
55 GHz Isolator	"	04/15/80	825
U-Band Waveguide Components	"	03/15/80	4,040
		TOTAL	$131,360

TABLE 6-II. FINANCIAL STATEMENT FROM THE NOVEMBER MONTHLY PROGRESS REPORT

Cost Information

The following charges have been incurred against the contract during the period 1 November to 30 November 1979.

Personal Services (PS)	$ 12,827.72
Materials and Supplies	84,987.25
Travel	1,367.70
Overhead (@ 76% of PS)	9,749.07
Retirement (@10.51% of PS)	1,321.43
TOTAL	$110,253.17

The breakdown of personal services is as follows:

	Dollars	Approximate Man Hours
Principal Research Engineers	$ 533.23	25
Senior Research Engineers	3,573.32	202
Research Engineers	5,676.49	425
Assistant Research Engineers	1,225.30	113
Student Assistants	254.60	48
Technicians, Machinists	1,474.97	170
Clerical	89.81	15
TOTAL	$12,827.72	998

The current financial status of the contract is as follows:

	Budget As Proposed	Expended	Free Balance
Personal Services (PS)	$ 28,558	$ 23,171.39	$ 5,386.61
Materials and Supplies	95,897	118,740.00	-22,843.00
Travel	440	1,939.56	- 1,499.56
Computer	400	0.00	400.00
Overhead	21,704	17,610.26	4,093.74
Retirement	3,001	2,386.69	614.31
AS PROPOSED	$150,000	$163,847.90	-$13,847.90*

* Based on present partial funding, the funding and equivalent man hours are sufficient to complete the task. Approximately 8% of the proposed task has been completed. Additional funds have been allocated for FY-80, and will offset the overrun for materials and supplies.

The financial status of the program is good at the present time, but a potential problem area in materials and supplies (M&S) must be pointed out. A low estimate on the cost of the gimbal system together with some unanticipated expenses for microwave components cause the M&S estimate to increase from $128,125, given in the proposal to $178,572. This potential overrun will be divided among the various program subtasks in an attempt to cover it with existing funds. Every effort will be made to ensure that no additional funds are required.

REFERENCES

1. R. G. Shackelford and J. J. Gallagher, "Millimeter Wave Beamrider System", U. S. Army MIRADCOM Technical Report TE-CR-77-7, Army, 1977.

2. P. S. Henry, "Frequency Agile Millimeter-Wave Phase Lock System", Rev. Sci. Instrum., 47, 9, Sept. 1976, pp. 1020-1025.

3. R. G. Strauch, W. T. Smith, and V. E. Derr, "Injection Locking of a Laddertron at 35 Gc/s", IEEE Trans. Microwave Theory Tech., Vol. MTT-13, July 1965, pp. 473-474.

4. R. E. Forsythe, V. T. Brady, and G. T. Wrixon, "Development of a 183 GHz Subharmonic Mixer", IEEE-MTT Symposium, Orlando, Fla., May 1974.

5. A. Saleh, "An Adjustable Quasi-Optical Bandpass Filter - Part I: Theory and Design Formulas", IEEE Trans. Microwave Theory Tech., Vol. MTT-22, No. 7, July 1974, pp. 728-734.

6. _____, "An Adjustable Quasi-Optical Bandpass Filter - Part II: Practical Considerations", Ibid, pp. 734-739.

7. R. D. Hayes, "95 GHz Pulsed Radar Returns From Trees", EASCON, October 1979.

8. N. C. Currie, D. J. Lewinski, M. S. Applegate and R. D. Hayes, "Radar Millimeter Backscatter Measurements", AFATL-TR-77-92, Vol. 1, July 1977.

9. M. I. Skolnik, Editor, Radar Handbook, McGraw-Hill, New York, 1970, Chapter 2.